

This is a repository copy of *Parallel fault detection algorithm for grid-connected photovoltaic plants*.

White Rose Research Online URL for this paper:

<https://eprints.whiterose.ac.uk/177679/>

Version: Accepted Version

---

**Article:**

Dhimish, Mahmoud, Holmes, Violeta and Dales, Mark (2017) Parallel fault detection algorithm for grid-connected photovoltaic plants. *Renewable Energy*. pp. 94-111. ISSN 0960-1481

<https://doi.org/10.1016/j.renene.2017.05.084>

---

**Reuse**

Items deposited in White Rose Research Online are protected by copyright, with all rights reserved unless indicated otherwise. They may be downloaded and/or printed for private study, or other acts as permitted by national copyright laws. The publisher or other rights holders may allow further reproduction and re-use of the full text version. This is indicated by the licence information on the White Rose Research Online record for the item.

**Takedown**

If you consider content in White Rose Research Online to be in breach of UK law, please notify us by emailing [eprints@whiterose.ac.uk](mailto:eprints@whiterose.ac.uk) including the URL of the record and the reason for the withdrawal request.

# Parallel Fault Detection Algorithm for Grid-Connected Photovoltaic Plants

Mahmoud Dhimish, Violeta Holmes, Mark Dales

Department of Computing and Engineering, University of Huddersfield, Huddersfield, United Kingdom

---

## *Abstract*

In this work, we present a new algorithm for detecting faults in grid-connected photovoltaic (GCPV) plant. There are few instances of statistical tools being deployed in the analysis of PV measured data. The main focus of this paper is, therefore, to outline a parallel fault detection algorithm that can diagnose faults on the DC-side and AC-side of the examined GCPV system based on the t-test statistical analysis method. For a given set of operational conditions, solar irradiance and module's temperature, a number of attributes such as voltage and power ratio of the PV strings are measured using virtual instrumentation (VI) LabVIEW software.

The results obtained indicate that the parallel fault detection algorithm can detect and locate accurately different types of faults such as, faulty PV module, faulty PV String, Faulty Bypass diode, Faulty Maximum power point tracking (MPPT) unit and Faulty DC/AC inverter unit. The parallel fault detection algorithm has been validated using an experimental data climate, with electrical parameters based on a 1.98 and 0.52 kWp PV systems installed at the University of Huddersfield, United Kingdom.

**Keywords:** *Photovoltaic System, Photovoltaic Faults, Fault Detection, LabVIEW*

---

## *1. INTRODUCTION*

In recent years the photovoltaic market has developed rapidly throughout the world. A significant factor leading to this large growth in the PV industry is the reduction of PV generation costs. In addition, most developed countries have implemented specific governmental strategies to encourage the introduction of grid connected PV plants. Successful examples can be seen in Germany, Japan and Kenya [1]. This important growth has not, however, been accompanied by similarly significant improvements in the field of PV system fault diagnosis and detection. Most PV systems, currently in use, operate without any supervisory mechanism. These tend to be PV systems with power outputs below 25 kWp [2]. However, following the fast growth of PV installations, fault detection techniques nowadays are important to be deployed in smaller scale PV systems which do tend to be 25KWp or less.

The need for higher performance, efficiency and reliability for grid-connected PV (GCPV) systems has led to a recent interest in fault detection algorithms. Different factors can be responsible for the production losses in a PV system, including; maximum power point tracking (MPPT) error [3-4], wiring losses and ageing [5], shading effect [6-7], dust effect [8], snow accumulation on the surface of the solar panels [9] and faulty dc-ac inverters [10].

There are existing techniques which have been developed for fault detection in grid connected PV plants. Some use satellite data [11] for fault detection using GITEL approach which facilitate the detection of several faulty conditions in PV systems such as partial shading effect, faulty PV modules and faulty PV

40 string. However, some algorithms do not require any climate data (Solar irradiance and module  
41 temperature) but instead use earth capacitance measurements in a technique established by Takashima et  
42 al [12], this approach follows three PV performance diagnosis layers, starting with passive diagnosis part,  
43 then fault separation method and ending with active layer which contains the fault location in a PV string.

44 Other fault detection algorithm techniques are based on a diagnostic signal which indicates a possible  
45 fault occurring in the GCPV plant such as short circuit fault in any bypass diodes in PV string, shunted  
46 bypass diode fault and connection resistance fault between PV modules [13]. In [14], the authors  
47 proposed a reliable fault detection method for grid-connected PV plants. The method was developed  
48 using two algorithms based on artificial neural network (ANN) and I-V characteristics of the examined  
49 PV system.

50 The development of a fault detection algorithm which allows the detection of seven different fault modes  
51 on the DC-side of a GCPV system is presented by M. Dhimish & V. Holmes [15]. The algorithm uses the  
52 t-test statistical approach for identifying the presence of system fault conditions. However in [16], the  
53 fault detection algorithm focuses on the AC-side of the GCPV system. The approach uses the  $\pm 3$  standard  
54 deviation statistical analysis technique. Hot-spot detection in photovoltaic substrings using AC  
55 parameters characterization was developed by [17], this approach is used to detect the number of shaded  
56 modules in a PV string, moreover, and the algorithm proves that the hot spot detection can be achieved  
57 with two frequency measurements: one for the higher frequency capacitive region and one for the low  
58 frequency dc impedance region. Nevertheless, the analysis of the current and voltage indicators in a  
59 GCPV system operating in partial shading faulty conditions is created by Silvestre et al [18], this  
60 approach is using the relationship between the ratios of the current in case of one faulty string and fault-  
61 free operation mode. In addition to the ratio between the voltage ratios in case of one bypassed PV  
62 module and fault-free operation mode.

63 In this work, we present the development of a fault detection algorithm which allows the parallel  
64 detection of faults occurring on both the DC and AC sides of the examined GCPV plant. The algorithm  
65 uses the theoretical and measured power outputs from the GCPV plant. Initially, the measured output  
66 power is compared with the theoretical power. Subsequently, a statistical t-test technique is used to check  
67 the location of the fault which has occurred on the system. Two parameters are calculated and used in  
68 order to determine the type of fault: The power ratio between the simulated and measured power (PR);  
69 and the ratio between the simulated and measured voltage (VR).

70 The algorithm was developed and validated using online and historical field measurements from a 1.98  
71 kWp PV plant located in Huddersfield, United Kingdom. The parallel fault detection algorithm was  
72 validated with data that include measurements taken during the faulty operation of the GCPV plant. Fig.  
73 1 shows all types of faults which can be identified by the proposed parallel fault detecting algorithm. It  
74 can be observed that faults occurring in GCPV plants can be classified into three main categories:

- 75 • Faults in the data acquisition
- 76 • Faults in the DC-side of the GCPV system
- 77 • Faults in the AC-side of the GCPV system

78 A software tool is designed using Virtual Instrumentation (VI) LabVIEW to automatically display and  
79 monitor the possible faults occurring within the GCPV plant. A LabVIEW VI is also used to log the  
80 measured power, voltage and current data for the entire GCPV system.

81 The main contribution of this work is the development and implementation of a simple, fast and reliable  
82 fault diagnosis algorithm for GCPV plants. The statistical t-test method is used to determine the location

83 of the fault in the PV system, there is, therefore, no requirement to compare the measured data with a  
 84 specific simulation threshold as described in [13, 14 and 16]. In practice, the parallel detection algorithm  
 85 is capable of localizing and identifying faults occurring in: A PV module in a PV string; Two PV modules  
 86 in a PV string; A faulty PV string; A Faulty MPPT; Shading effect with faulty bypass diodes; A faulty  
 87 DC/AC inverter unit and; Data acquisition errors. Fault data analysis is performed using two algorithms  
 88 operating in parallel:

- 89 • Algorithm 1, is implemented to detect faults in the DC-side of the GCPV plant
- 90 • Algorithm 2, is implemented to detect faults in the AC-side of the GCPV plant

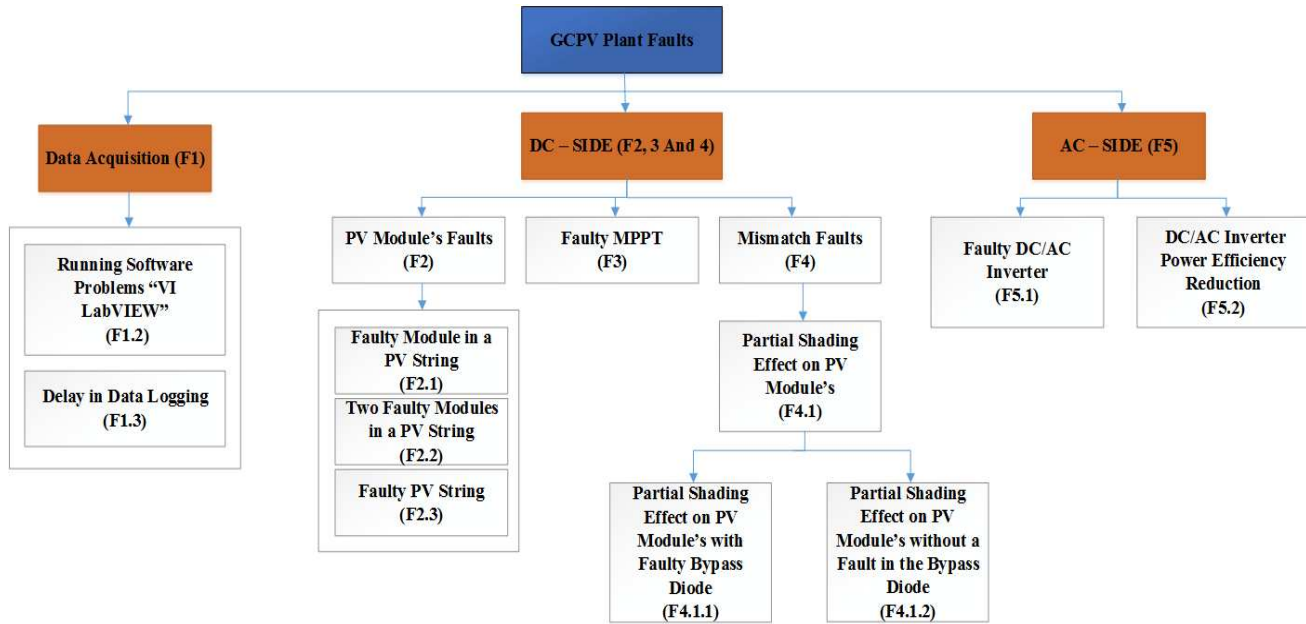


Fig. 1. Different Type of Faults Occurring in the examined GCPV Plant

91 This paper is organized as follows: Section 2 presents the data acquisition in the GCPV plant. Section 3  
 92 describes the methodology used, Fault detection algorithm and diagnosis rules are presented, while  
 93 section 4 lists the results and discussion of the work. Finally, section 5 describes the conclusion and future  
 94 work.

## 95 2. GCPV PLANT AND DATA ACQUISITION

96 The PV system used in this work comprises a grid-connected PV plant containing 9 polycrystalline  
 97 silicon PV modules each with a nominal power of 220 Wp. The photovoltaic modules are organized in 3  
 98 strings and each string is made up of 3 series-connected PV modules. Using a photovoltaic connection  
 99 unit which is used to enable or disable the connected of any PV modules from the entire GCPV plant,  
 100 each photovoltaic string is connected to a Maximum Power Point Tracker (MPPT) which has an output  
 101 efficiency not less than 98.5%. subsequently, each MPPT unit is connected to a DC/AC inverter unit  
 102 manufactured by Victron Energy. The efficiency of the DC/AC unit is in the range 94% to 88%. The DC  
 103 current and voltage are measured using the internal sensors which are part of the Flexmax MPPT unit and  
 104 DC/AC inverter.

105 A Vantage Pro monitoring unit is used to receive the global solar irradiance measured by a Davis Weather  
 106 Station which includes a pyranometer. The Hub 4 communication manager is used to facilitate the

107 acquisition of module temperatures using the Davis external temperature sensor, and the electrical data  
 108 for each photovoltaic string. Finally, VI LabVIEW software is used to implement the data logging and  
 109 monitoring functions of the GCPV system. Fig. 2 illustrates the overall system architecture of the GCPV  
 110 plant.

111 The SMT6 (60) P solar module manufactured by Romag has been used in this work. The tilt angle of the  
 112 GCPV plant installation is 42°. The electrical characteristics of the solar module are shown in Table 1.  
 113 Additionally, the standard test condition (STC) for these solar panels are: Solar Irradiance= 1000 W/m<sup>2</sup>  
 114 And Module Temperature = 25 °C.

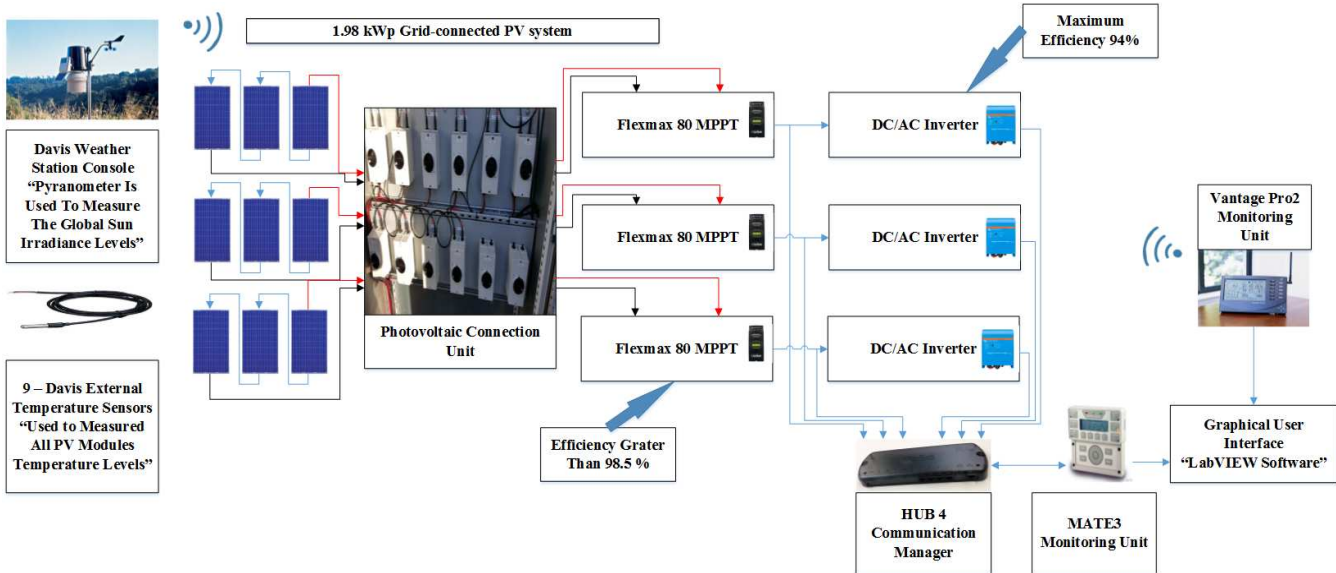


Fig. 2. The GCPV Plant Installed at the Huddersfield University, United Kingdom

TABLE 1  
 ELECTRICAL CHARACTERISTICS OF SMT6 (60) P PV MODULE

Solar Panel Electrical Characteristics	Value
Peak Power	220 W
Voltage at maximum power point ( $V_{mp}$ )	28.7 V
Current at maximum power point ( $I_{mp}$ )	7.67 A
Open Circuit Voltage ( $V_{OC}$ )	36.74 V
Short Circuit Current ( $I_{sc}$ )	8.24 A
Number of cells connected in series	60
Number of cells connected in parallel	1
$R_s, R_{sh}$	0.53 Ohms , 1890 Ohms
dark saturation current ( $I_o$ )	$2.8 \times 10^{-10}$ A
Ideal diode factor (n)	1.5
Boltzmann's constant (K)	$1.3806 \times 10^{-23}$ J.K <sup>-1</sup>

115 **3. METHODOLOGY**

116 **3.1. DC and AC Output Modelling**

117 The DC side of the GCPV system is modelled using 5-parameters model. The voltage and current  
 118 characteristics of the PV module can be obtained using the single diode model [19] as the following:

119 
$$I = I_{ph} - I_o \left( e^{\frac{V+IR_s}{nsV_t}} - 1 \right) - \left( \frac{V+IR_s}{R_{sh}} \right) \quad (1)$$

120 Where  $I_{ph}$  is the photo-generated current at STC,  $I_o$  is the dark saturation current at STC,  $R_s$  is the  
 121 module series resistance,  $R_{sh}$  is the panel parallel resistance,  $ns$  is the number of series cells in the PV  
 122 module and  $V_t$  is the thermal voltage and it can be defined based on:

123 
$$V_t = \frac{nKT}{q} \quad (2)$$

124 Where  $A$  the ideal diode factor,  $k$  is Boltzmann’s constant and  $q$  is the charge of the electron.

125 The five parameter model is determined by solving the transcendental equation (1) using Newton-  
 126 Raphson algorithm [20] based only on the datasheet of the available parameters shown previously in  
 127 Table 1. The power produced by PV module in watts can be easily calculated along with the current (I)  
 128 and voltage (V) that is generated by equation (1), therefore,  $P_{theoretical} = IV$ .

129 The Power-Voltage (P-V) curve analysis of the tested PV module is shown in Fig. 3. The maximum  
 130 power and voltage for each irradiance level under the same temperature value can be expressed by the P-  
 131 V curves. The purpose of using the analysis for the P-V curves, is to generate the expected output power  
 132 of the examined PV module, therefore, it can be used to predict the error between the measured PV data  
 133 and the theoretical power and voltage performance, this method is used with all examined PV modules.

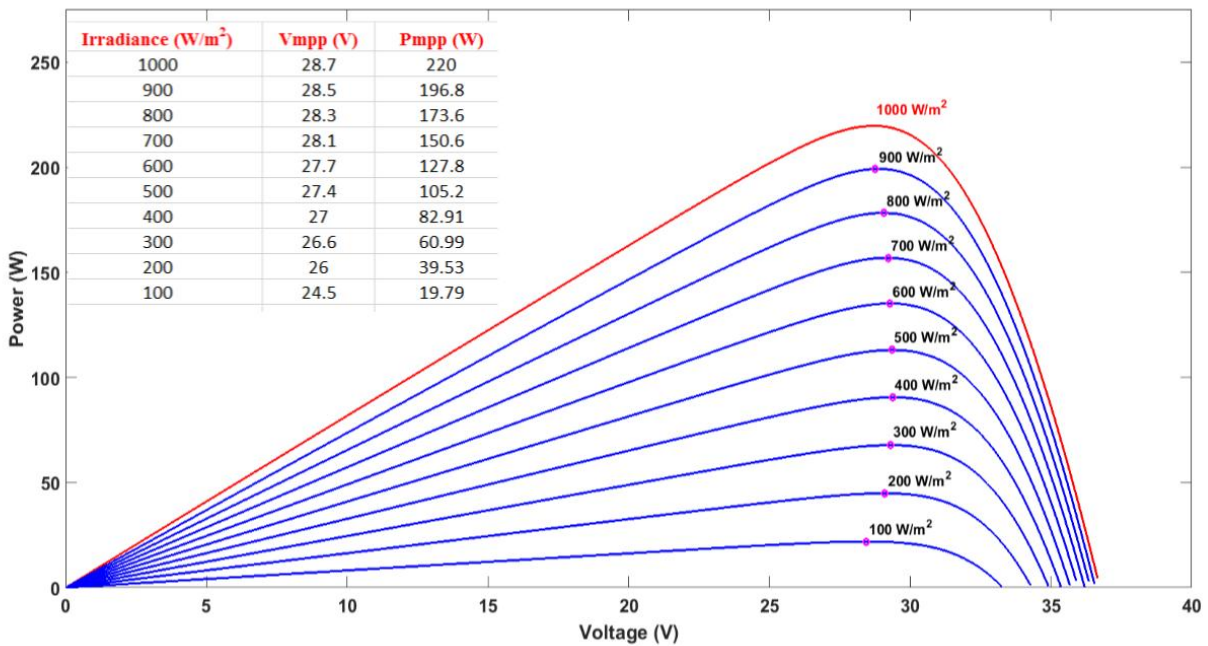


Fig. 3. Power-Voltage (P-V) curve modelling under various irradiance levels

134 The efficiency of an inverter converting the DC current and voltage into the AC Current and voltage has  
 135 been modelled with the standard approach given by [21]. The DC/AC inverter units which are used in this  
 136 work have a theoretical maximum and minimum conversion efficiency limits of 94% and 88%  
 137 respectively. The algorithm is using the max and the min thresholds of the conversion ratios for the  
 138 DC/AC inverter, therefore, the algorithm could be adapted with a different DC/AC inverter which has  
 139 different conversion limits.

140 Based on the output of the MPPT units, VI LabVIEW software is used to simulate the theoretical  
 141 thresholds for the DC/AC inverters, the power ratio of the DC/AC unit can be calculated using the  
 142 following:

$$143 \quad AC \text{ Power Ratio} = \frac{\text{Output AC Power}}{\frac{\text{Rated DC Power} \times \text{Total Insolation}}{\text{Irradiance Level}}} \quad (3)$$

144  
 145 Where rated DC power = the DC power at STC, Total insolation = total solar energy received by the PV  
 146 system over interval of time which the AC power ratio is calculated.  
 147  
 148

### 149 **3.2. GCPV Parallel Fault Detection Approach**

150 The main objective of the parallel fault detection algorithm is to detect and determine when and where a  
 151 fault has occurred in the examined GCPV plant. The algorithm uses the climate data that is collected  
 152 using the Davis weather station and the internal sensors of the MPPT and the DC/AC inverter unit.  
 153 Furthermore, LabVIEW software simulates the I-V and P-V theoretical curves of the GCPV system as  
 154 shown in Fig. 4(A).

155 The t-test statistical analysis method is used to compare the theoretical and measured output power of the  
 156 GCPV system. The t-test is evaluated using (4) where  $\bar{x}$  is the mean of the samples,  $\mu$  is the population  
 157 mean, n is the sample size and SD is the standard deviation of the entire data. The real-time  
 158 measurements are taken by averaging 60 samples taken at 1 second intervals. The results obtained for  
 159 power, voltage and current are calculated at one minute intervals for each sample set. To determine  
 160 whether the t-test analysis is significant, a threshold value of 2.68 was used as shown in Fig. 4(B).

161 The parallel fault detection algorithm will be activated if the value of the t-test is higher than 2.68. Fig.  
 162 4(C) describes the parallel fault detection algorithm, which contains two different algorithms:

163 Algorithm 1, is used to diagnosis the faults on the DC-side of the GCPV system. This algorithm can  
 164 detect multiple faults such as:

- 165 • Faulty PV module in a PV string And Two faulty PV modules in a PV string
- 166 • Faulty PV String
- 167 • Partial Shading (PS) with and without faulty bypass diodes in the PV string
- 168 • Faulty MPPT

169 Algorithm 2, is used to detect the faults on the AC-side of the GCPV system. There are two faults that can  
 170 be detected using this algorithm: faulty DC/AC inverter or output power efficiency reduction in the  
 171 DC/AC inverters. Faulty data acquisition is detected if there is a delay in the data logging or a faulty  
 172 simulation by the VI LabVIEW software.

$$173 \quad t = \frac{(\bar{x} - \mu)\sqrt{n}}{SD} \quad (4)$$

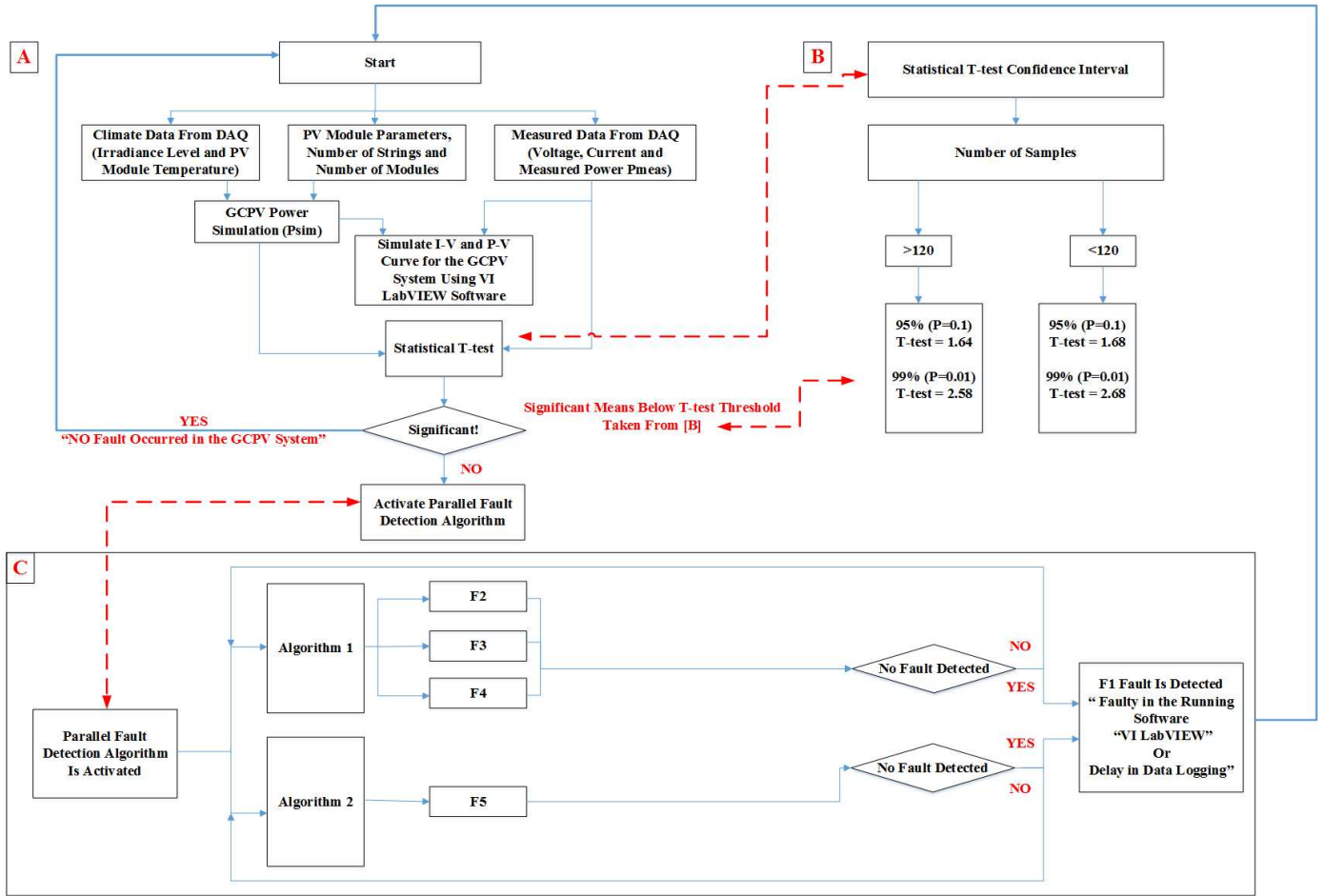


Fig. 4. Fault Detection in the GCPV Plant. (A) General Algorithm Using T-test Statistical Technique, (B) T-test Statistical Confidence Interval Limits, (C) Parallel Fault Detection Algorithm

### 3.3. Fault Detection Algorithm 1

174 Fault detection algorithm 1 is used to determine the type of fault occurred on the DC-side of the examined  
 175 GCPV system. Two ratios have been identified. Power ratio (PR) and voltage ratio (VR) have been used  
 176 to categorize the region where the fault has occurred. Both ratios can be calculated using the following  
 177 expressions:

$$178 \quad PR = \frac{P_{theoretical}}{P_{measured} \times MPPT \text{ efficiency}} \quad (5)$$

$$179 \quad VR = \frac{V_{theoretical}}{V_{measured} \times MPPT \text{ efficiency}} \quad (6)$$

180 Where  $P_{theoretical}$  is the theoretical output power generated by the GCPV system,  $P_{measured}$  is the  
 181 measured output power from PV string,  $V_{theoretical}$  is the theoretical output voltage generated by the  
 182 GCPV system and  $V_{measured}$  is the measured output DC voltage from PV string.

183 Based on the analysis of the PR for the GCPV system, numerical calculations for the DC-side fault rules  
 184 is expressed in Fig. 5. Since the internal sensors of the MPPT have a conversion error rate of 98.5%, the  
 185 power ratios are calculated at 1.5% error tolerance of the theoretical power which presents the maximum  
 186 error condition for the examined GCPV system. The values are calculated according to the set of  
 187 conditions shown in Fig. 5.

188 The voltage ratios are used to identify the fault type occurring in the GCPV system. Fig. 6 describes the  
 189 relationship between the power ratios and voltage ratios. Faults can be detected according to the following  
 190 conditions:

- 191 1) Sleep mode will start during the night when  $PR=0$ .
- 192 2) If  $1.015228 \geq PR \geq 1$ : it means that the GCPV system operates at the normal operation mode.
- 193 3) If  $1.5233 \geq PR \geq 1.5$ : in this case two categories of faults can be identified: if  $2.47445 \geq VR \geq$   
 194  $1.5$ : It indicates that there is a faulty PV module in the string, otherwise, a partial shading  
 195 condition has occurred in the PV string.
- 196 4) If  $3 > PR > 1.5223$ : in this case if the voltage ratio is between 2.47445 and 1.5, a faulty PV  
 197 module and a partial shading effect on the PV string has arisen. However, if the voltage ratio is  
 198 outside of the range 2.47445 - 1.5, partial shading is the only condition affecting the PV string.
- 199 5) If  $1000 > PR \geq 3$ : This case can determine various faults such as: Faulty PV module with PS  
 200 effect on the PV string, partial shading effect on the PV string, two faulty modules in the PV  
 201 string, two faulty modules in the PV string and partial shading effect.
- 202 6) If  $PR = 1000$ , where the GCPV plant has a failure in a PV string or a failure in a MPPT unit.

203 The theoretical short circuit current  $I_{sc}$  of the GCPV system is 8.18A. For all partial shading conditions if  
 204 the measured short circuit current is less than 98.5% of the theoretical short circuit value which is equal to  
 205 8.0573A, a faulty bypass diode has been detected in the GCPV system, this is acknowledged by shading  
 206 identification region (SIR) in Fig. 6.

207 The decision between any cases are illustrated in Fig. 6, for example, when a power ratio (PR) is equal to  
 208 1.5, the algorithm has to decide the fault type, which leads to specify the measured voltage ratio (VR).  
 209 Therefore, if the VR is between 2.47 and 1.5, faulty photovoltaic module is detected in the GCPV plant  
 210 otherwise, partial shading has been occurred as specified by SIR identification region.

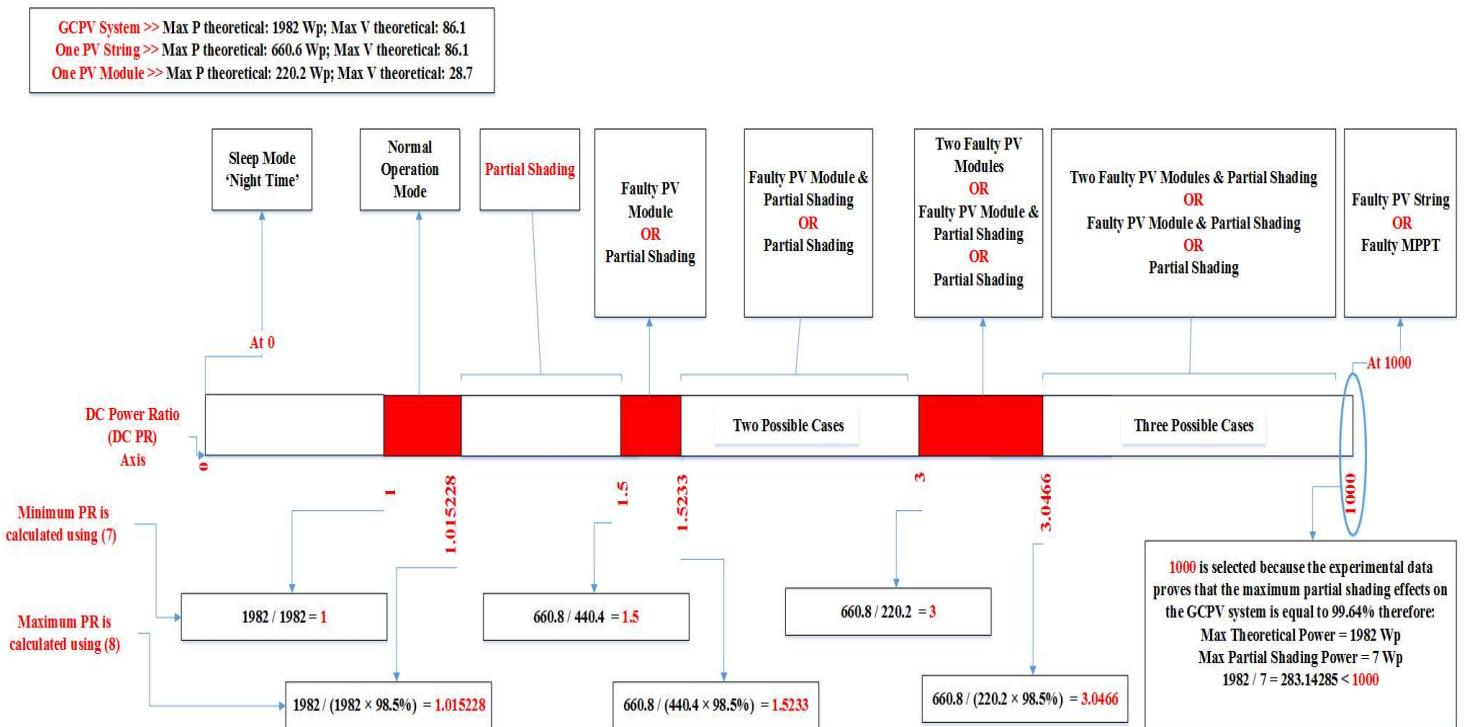


Fig. 5. Diagnosis the Faults in the DC-Side of the GCPV Based on the Power Ratios Rule

211 It is expected that fault detection algorithm 1 can be used on GCPV plants. By applying, (5) for the power  
 212 ratio calculations and, (6) for the voltage ratio calculations, it is possible to generate a fault detection rule.  
 213 Moreover, fault condition regions strongly depend on the number of modules present in each PV string.  
 214 In this work, all calculations are based on the use of three module PV strings. Therefore, in order to apply  
 215 the first algorithm, for fault detection on the DC-side of the GCPV system, it is necessary to consider the  
 216 percentage of MPPT error and the number of modules in each PV string.

217 The estimate for the maximum percentage error varies from one GCPV plant to another. A value of  
 218 98.5% has been used as a maximum, in this case, because the MPPT generates a measured power greater  
 219 than 98.5% of the theoretical simulated power. Hence, the maximum measured error tolerance for the  
 220 voltage and power ratio can be evaluated accurately up to 1.5%. In order to make this rule applicable to  
 221 other GCPV plants, it is necessary to use the percentage of MPPT error for that particular plant.

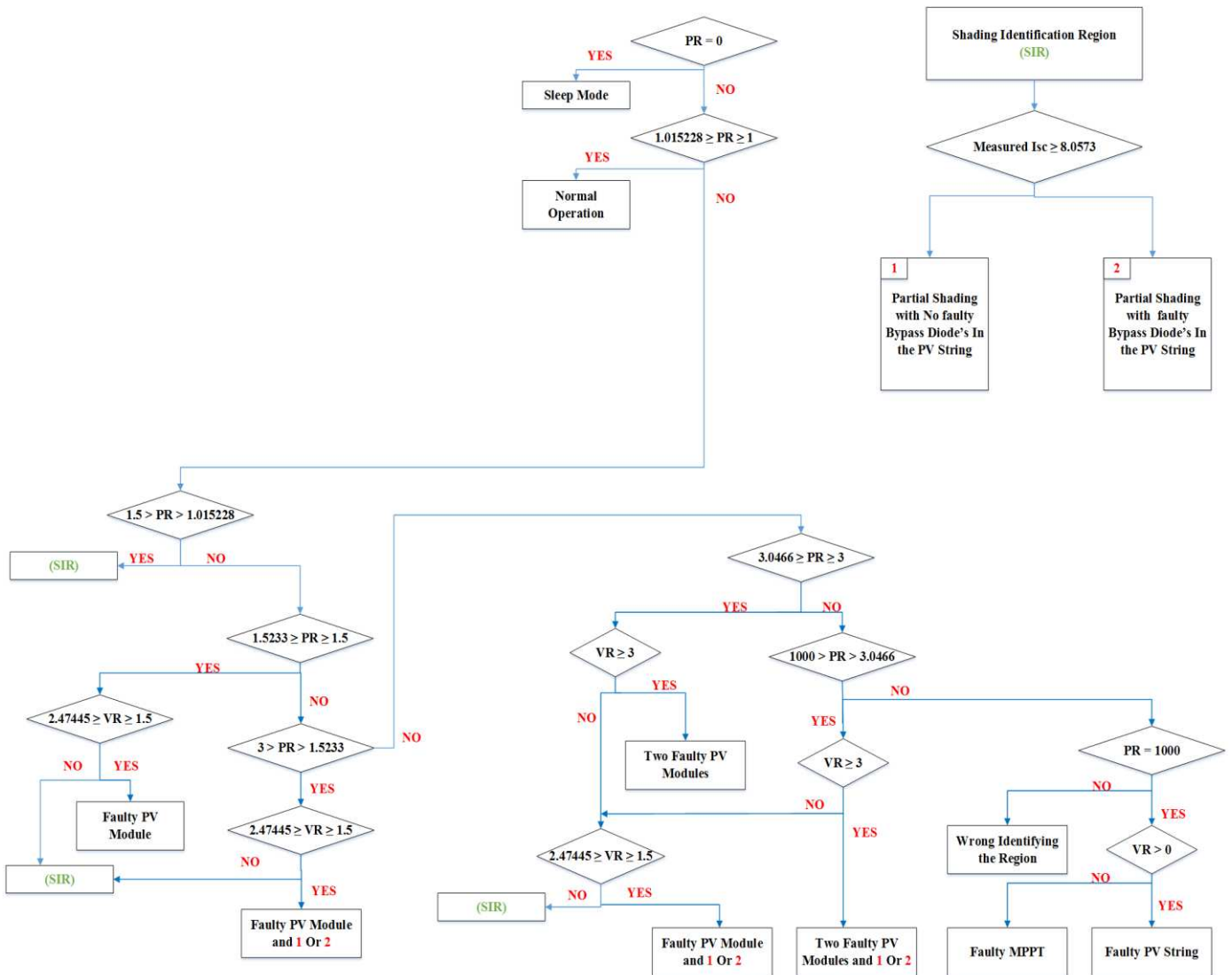


Fig. 6. Diagnosis the error in the DC-Side Faulty Conditions Based on The Voltage and Power Ratios

222 **3.5. Fault Detection Algorithm 2**

223 Fault detection algorithm 2, is used to detect two different fault types which occur in the DC/AC inverter units:  
224 units:

- 225 • Faulty DC/AC inverter unit: indicating that the DC/AC unit has stopped working.
- 226 • Reduction in the output power efficiency of the DC/AC inverter unit: indicating that the DC/AC inverter unit has reached an output power efficiency of less than 88%.

228 It is known that most AC inverters has an automatic disconnection to avoid islanding and other internal  
229 protection. However, many AC inverters are not capable to display the type of the fault occurred.  
230 Therefore, algorithm 2 was made to display for the end user two different faulty conditions which might  
231 occur in the AC inverters used in PV installation. This feature is useful for maintenance requirements and  
232 to monitor the performance of the AC side for the GCPV plant.

233 The datasheet for the DC/AC inverter unit shows the maximum output power efficiency to be 94% and  
234 the minimum to be 88%. Under standard test condition (STC), the theoretical output power of a PV  
235 string in the GCPV system is equal to 660.8 Wp and the maximum error tolerance of the MPPT is equal  
236 to 1.5%. Therefore, the normal operation limits for the DC/AC inverter units can be evaluated between  
237 AC power ratios (AC PR) in the range 1.0648 - 1.1387 as shown in Fig. 7.

238 If  $1000 > PR_{AC} > 1.1387$ , the DC/AC unit has a reduction in the output power efficacy. However, if the  
239  $PR_{AC} \geq 1000$ , it means that the DC/AC inverter unit has stopped working indicating a faulty DC/AC  
240 unit. A numerical value of 1000 was selected as an upper threshold because experimental data proves that  
241 the maximum output power efficiency reduction in the DC/AC inverter unit is equal to 1.3%. Therefore,  
242  $650.888 / 8.461544 = 76.923076$  which is less than 1000.

243 It is possible to apply fault detection algorithm 2 in other GCPV plants. The only requirements for this  
244 algorithm are, the MPPT error tolerance rate, and the maximum/minimum output power efficiency for the  
245 examined DC/AC invert unit. For further investigations, this algorithm can be adapted to be used with  
246 various GCPV system architecture implementations such as a central inverter configuration [23] and a  
247 module integrated inverter configuration [24].

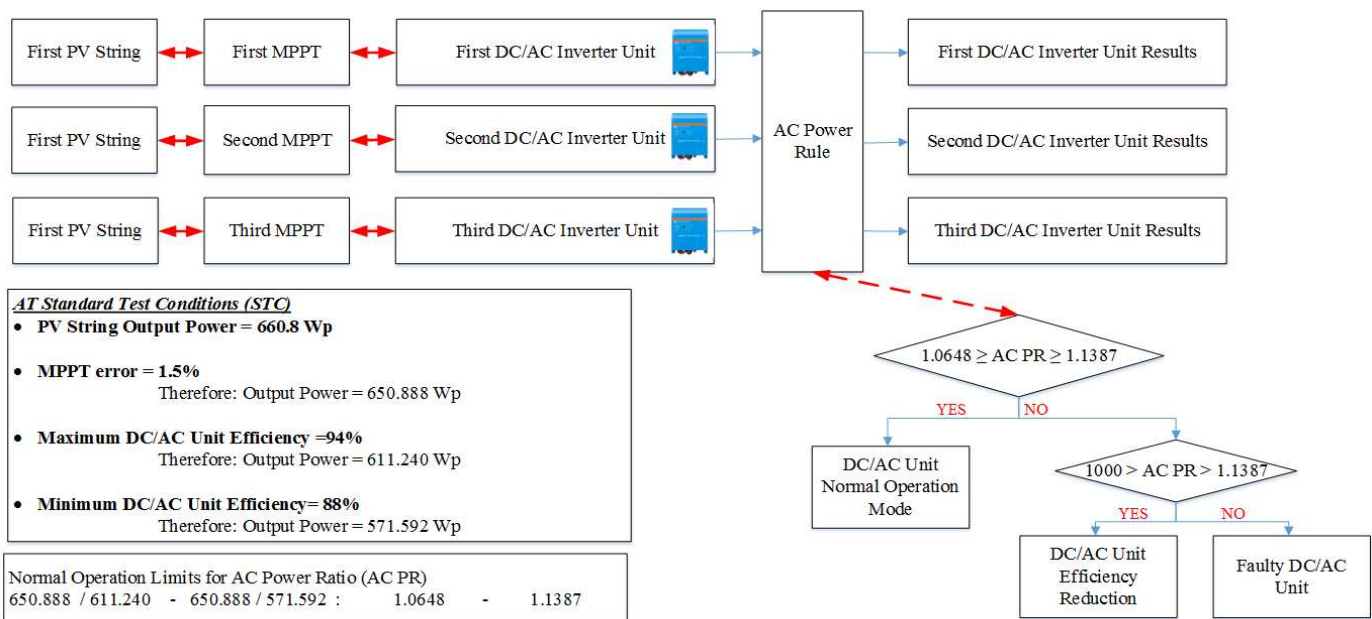


Fig. 7. Diagnosis the Faulty Conditions in the AC-Side Based on Power Ratios

248 **4. RESULTS AND DISCUSSION**

249 In this section, the performance of the parallel fault detection algorithm is verified. Four different sub-  
250 sections are demonstrated: the normal operation and sleep mode, diagnosis the faults in the data  
251 acquisition, performance evaluation for the fault detection algorithm 1 and algorithm 2. The acquired data  
252 for various days have been considered. The time zone for all measurements is GMT.

253 **4.1. Normal Operation and Sleep Mode**

254 The Normal operation and sleep mode for the GCPV system is shown in Fig. 8. Starting from 6:00am and  
255 ending at 6:21am, the GCPV system is in sleep mode where the GCPV system has not yet received any  
256 solar irradiance to generate output power. However, between 6:22am and 19:41pm, the GCPV system is  
257 in the normal operation mode. The measured DC and AC power is very close to the theoretical DC and  
258 AC output power. According to the achieved results of this test, the output power efficiency for both the  
259 DC/DC converter and DC/AC inverter is equal to 98.89% and 92.7% respectively. Fig. 8 shows that the  
260 GCPV system is stable for all variation of the measured sun irradiance levels.

261 **4.2. Diagnosis the Fault in the Data Acquisition**

262 There are multiple possible faults that may occur in the GCPV system due to the data acquisition units  
263 such as:

- 264 • Running VI LabVIEW software: errors in loading graphs, errors in saving data.
- 265 • Delay in Data Logging: faulty in the internal sensors of the DC/DC or DC/AC units.

266 As shown in Fig. 9, the VI LabVIEW software stopped logging the measured and theoretical data  
267 between 13:27pm and 13:55pm. This type of fault might occur in running software due to VI LabVIEW  
268 version updates and the multi functions which the software handles at the same time. It is therefore  
269 required to create a structural code format before the data collection step.

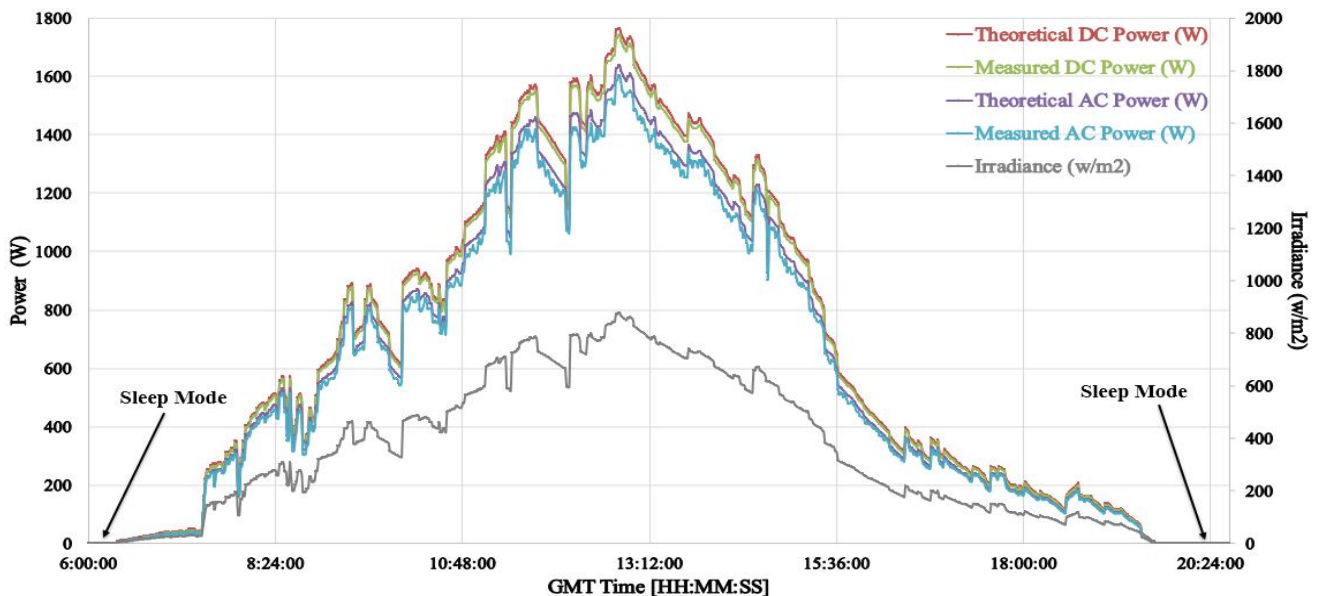


Fig. 8. GCPV System Theoretical and Measured Output DC and AC Power in a Normal Operation and Sleep Mode

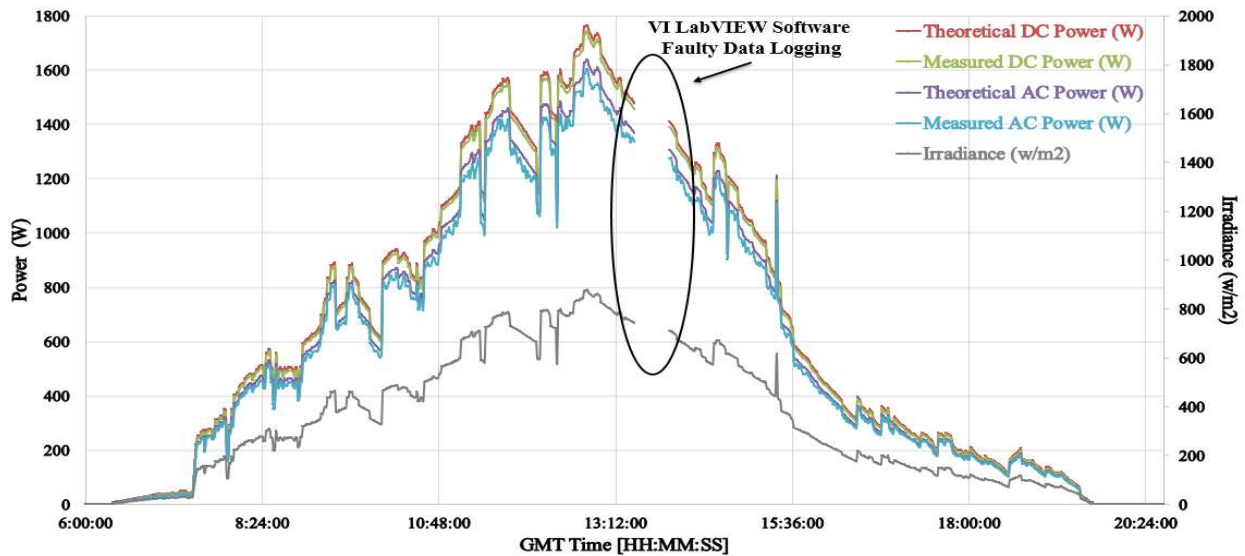


Fig. 9. Diagnosis the Fault in the Data Acquisition Due to Faulty Data Logging Using VI LabVIEW Software

#### 270 4.3. Performance Evaluation for Algorithm 1, DC-Side

271 In order to test the ability of the fault detection algorithm 1, described previously in section 3.3, a number  
 272 of experiments were conducted over a full day period. Table 2 shows the start and end times for each  
 273 experiment that has been examined in the GCPV system. Ten different case scenarios were tested  
 274 sequentially, between 6:00am and 20:24pm. Brief description on how the GCPV system was perturb is  
 275 shown in appendix A.

276 As shown in Fig. 10, starting from 6:21am, the GCPV system starts to generate output power after the  
 277 sleep mode is finished. The GCPV system operates in a normal operation mode until 10:00:18am, where  
 278 the power ratio and the voltage ratio of this case are equal to 1.012 and 1.18 respectively as illustrated in  
 279 Figs. 10(A) and 10(B).

280 One faulty PV module test is conducted in the first PV string between 10:00:18am and 11:00:18am. The  
 281 PR and VR for this particular case are equal to 1.511 and 1.502 respectively. Two faulty PV modules in  
 282 the second PV string are tested between 11:00:18am and 12:00:18pm. In this case, the PR for the second  
 283 PV string is equal to 3.021, while the first and third PV strings operate in normal mode during the test  
 284 period.

285 By disconnecting one PV module and applying a 30% partial shading, using an opaque paper object, to  
 286 the third PV string as shown in Fig. 11(A) between 12:00:18pm and 14:00:18pm, the power ratio is equal  
 287 to 2.36. Additionally, the measured short circuit current is used to detect possible faults in the bypass  
 288 diode for the examined PV string. Fig. 11(C) shows the variation of the measured short circuit current for  
 289 the GCPV system. As described previously in section 3.3, the theoretical upper and lower limits for the  
 290 short circuit current are equal to 8.18 and 8.0571 respectively. A faulty bypass diode is detected by the  
 291 algorithm between 13:00:18pm and 14:00:18pm. In this case, the measured short circuit current lies  
 292 between 5.6A and 5.9A.

293 The only difference between an MPPT fault and a PV string fault is that during the latter the voltage ratio  
 294 maintains a value greater than 1. Faulty MPPT and faulty PV string situations are tested between  
 295 14:00:18pm and 16:00:18pm in different PV strings. The voltage and the power ratio for a faulty MPPT is  
 296 equal to 1000 for the first PV string as shown in Figs. 10(A) and 10(B). However, the power and voltage  
 297 ratio for the faulty PV string tested between 15:00:18pm and 16:00:18pm on the second PV string is equal  
 298 to 1000 and 1.003 respectively.

299 From 16:00:18pm until 20:24:00pm no faults occurred in the GCPV system and the sleep mode of the  
 300 system starts when the power ratio and voltage ratio is equal to zero at 19:41:18pm.

301 All obtained results for the various test conditions indicate that fault detection algorithm 1 has a high  
 302 detection capability: there is no evidence of any errors in the detecting algorithm while conducting  
 303 different fault case scenarios at different PV locations. The time, location and type of fault is recognized  
 304 by the algorithm.

TABLE 2  
 DIAGNOSIS MULTIPLE FAULTS IN MULTIPLE STRINGS LOCATIONS

Case Number	Start Time	End Time	First PV String	Second PV String	Third PV String
1	6:00:00 am	6:21:18 am	Sleep Mode	Sleep Mode	Sleep Mode
2	6:21:18 am	10:00:18 am	Normal Operation	Normal Operation	Normal Operation
3	10:00:18 am	11:00:18 am	Faulty PV Module	Normal Operation	Normal Operation
4	11:00:18 am	12:00:18 pm	Normal Operation	Two Faulty PV Modules	Faulty PV Module
5	12:00:18 pm	13:00:18 pm	Normal Operation	Normal Operation	30% Partial Shading and Faulty PV Module without Fault in Bypass Diode in the PV String
6	13:00:18 pm	14:00:18 pm	Normal Operation	Normal Operation	30% Partial Shading and Faulty PV Module and Faulty Bypass Diode in the PV String
7	14:00:18 pm	15:00:18 pm	Faulty MPPT	Normal Operation	Normal Operation
8	15:00:18 pm	16:00:18 pm	Faulty MPPT	Faulty PV String	Normal Operation
9	16:00:18 pm	19:41:18 pm	Normal Operation	Normal Operation	Normal Operation
10	19:41:18 pm	20:24:00 pm	Sleep Mode	Sleep Mode	Sleep Mode

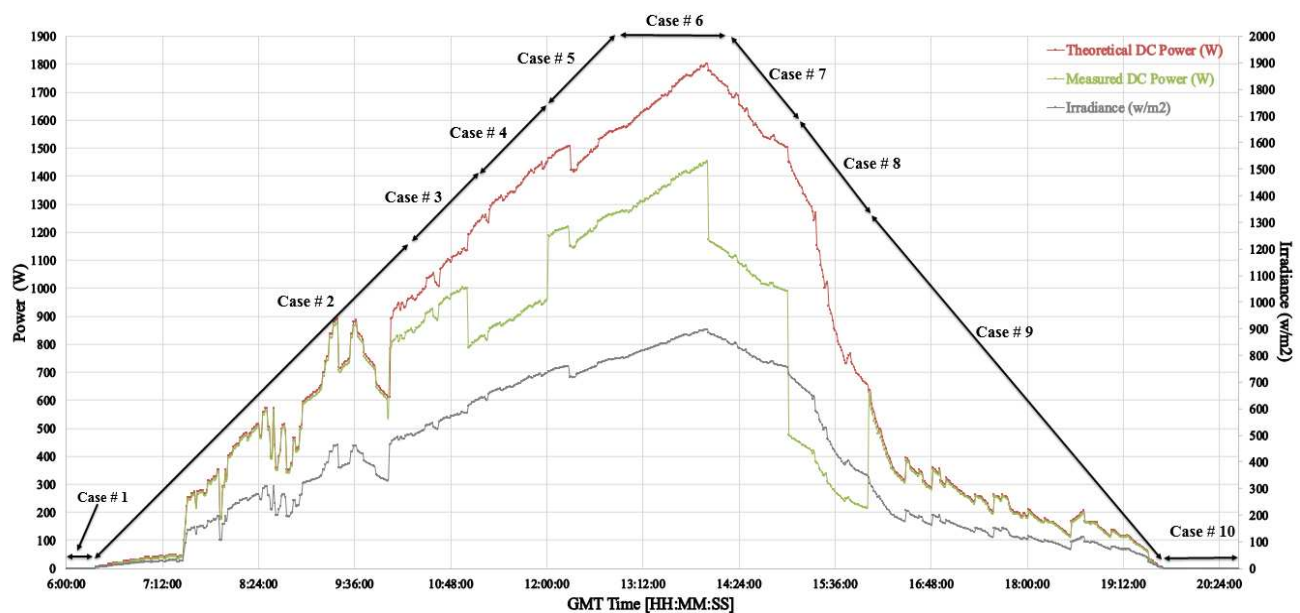
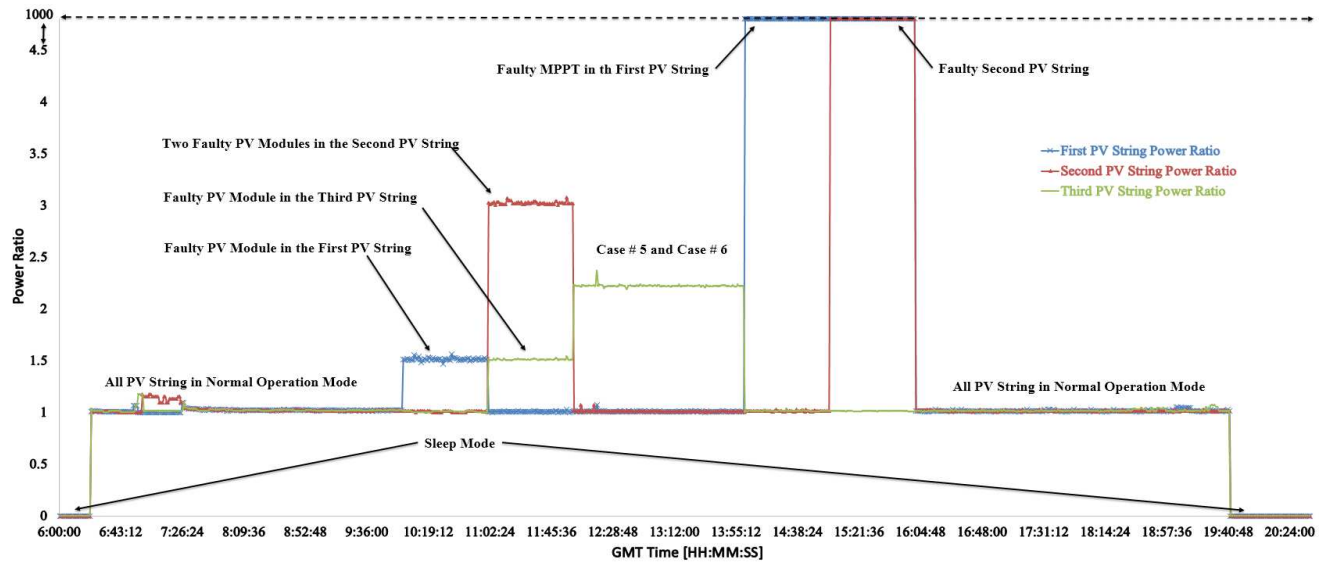
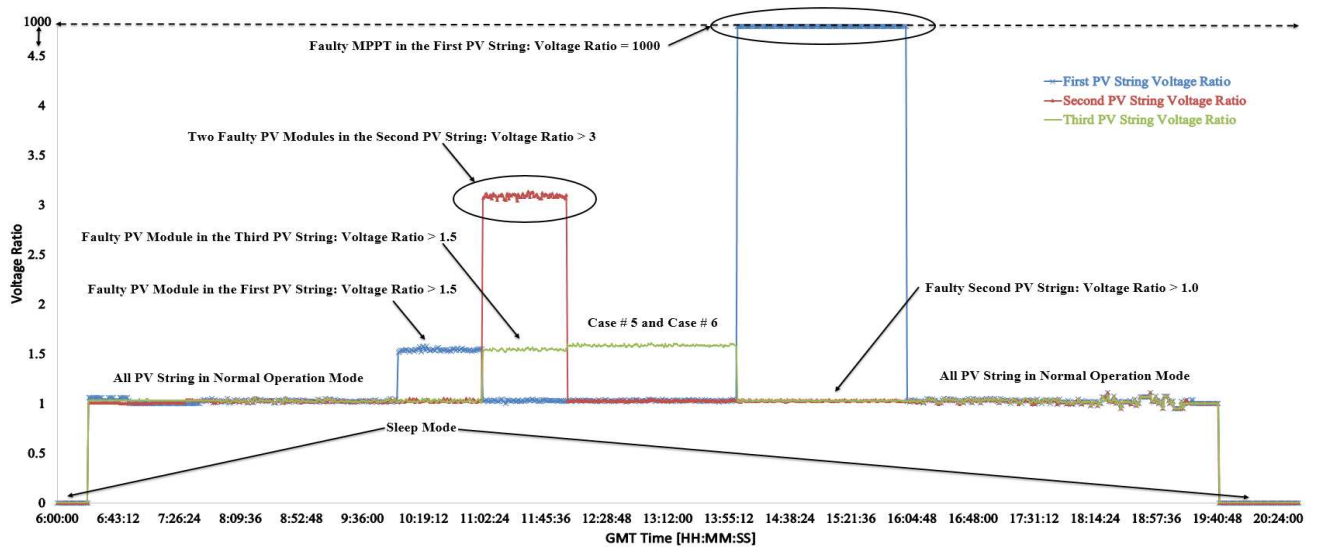


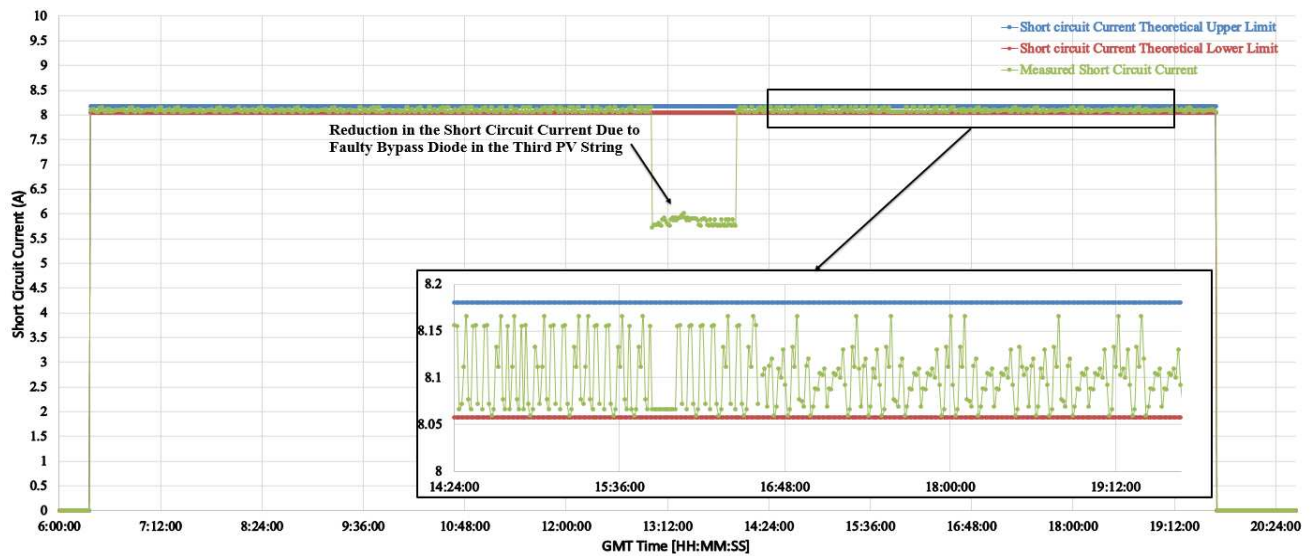
Fig. 10. GCPV System Theoretical DC Output Power vs. Measured Output DC Power Under 10 Different Case Scenarios



(A)



(B)



(C)

Fig. 11. Diagnosis the Faults Using Fault Detection Algorithm 1. (A) Power Ratio for all PV Strings, (B) Voltage Ratio for All PV Strings, (C) Measured Output Short Circuit Current Variations

305 **4.4. Performance Evaluation for Algorithm 2, AC-Side**

306 This section describes detection algorithm 2 which detects faults occurring on the AC-side of the GCPV  
 307 system. Table 3 illustrates the start and end times for each DC/AC inverter unit examined in the GCPV  
 308 system ten different case scenarios were tested sequentially between 6:00am and 20:24pm.

309 From 6:00am until 6:21:18am all DC/AC inverter units are in a sleep mode. The normal operation mode  
 310 for all DC/AC inverters is maintained between 6:21:18am and 10:00:18am. Moreover, Fig. 12(A) shows  
 311 all the variations of the output theoretical AC power vs. measured AC power.

312 A test with a faulty first DC/AC inverter unit, connected to the first PV String of the GCPV system, is  
 313 conducted between 10:00:18am and 11:00:18am. Fig. 12(B) shows that the power ratio for this scenario is  
 314 equal to 1000. The first and the second DC/AC inverter units are tested similarly under faulty operation  
 315 mode between 11:00:18am and 12:00:18pm; this scenario is represented as 5. During this scenario the  
 316 power efficiency for both faulty DC/AC inverter units is equal to 0, as shown in Fig. 12(C).

317 A reduction in output power efficiency, for the first DC/AC inverter unit, is examined between  
 318 14:00:18pm and 15:00:18pm. In this scenario, the efficiency of the DC/AC unit lies between 80% and  
 319 85%. However, the average power ratio is equal to 1.23 as shown in Fig. 12(B). This test has been  
 320 perturbed to the DC/AC inverters by7 reducing the conversion efficiency of the microcontrollers unit  
 321 embedded inside the inverters. There are many possible reasons for the reduction in the output power  
 322 efficiency for the DC/AC inverter units including:

- 323 • Efficiency reduction in the MPPT Unit connected directly to the DC/AC inverter unit [25].
- 324 • Partial shading conditions might affect the power ratios of the MPPT, with a consequent  
 325 reduction in output power efficiency of the DC/AC inverter unit [26].

326 In this section, algorithm 2, which detects faulty conditions in the AC-side of the GCPV system, is  
 327 examined. Algorithm 2 shows significant success in detecting any failure that occurs in any DC/AC  
 328 inverter unit. The time and the fault type can be identified using the fault detection algorithm.

TABLE 3  
 DIAGNOSIS MULTIPLE FAULTS IN MULTIPLE DC/AC INVERTER UNITS

Case Number	Start Time	End Time	First DC/AC Inverter Unit	Second DC/AC Inverter Unit	Third DC/AC Inverter Unit
1	6:00:00 am	6:21:18 am	Sleep Mode	Sleep Mode	Sleep Mode
2	6:21:18 am	10:00:18 am	Normal Operation	Normal Operation	Normal Operation
3	10:00:18 am	11:00:18 am	Faulty Inverter	Normal Operation	Normal Operation
4	11:00:18 am	12:00:18 pm	Normal Operation	Normal Operation	Normal Operation
5	12:00:18 pm	13:00:18 pm	Faulty Inverter	Faulty Inverter	Normal Operation
6	13:00:18 pm	14:00:18 pm	Normal Operation	Normal Operation	Normal Operation
7	14:00:18 pm	15:00:18 pm	Efficiency Reduction	Normal Operation	Normal Operation
8	15:00:18 pm	16:00:18 pm	Normal Operation	Normal Operation	Normal Operation
9	16:00:18 pm	19:41:18 pm	Normal Operation	Normal Operation	Normal Operation
10	19:41:18 pm	20:24:00 pm	Sleep Mode	Sleep Mode	Sleep Mode

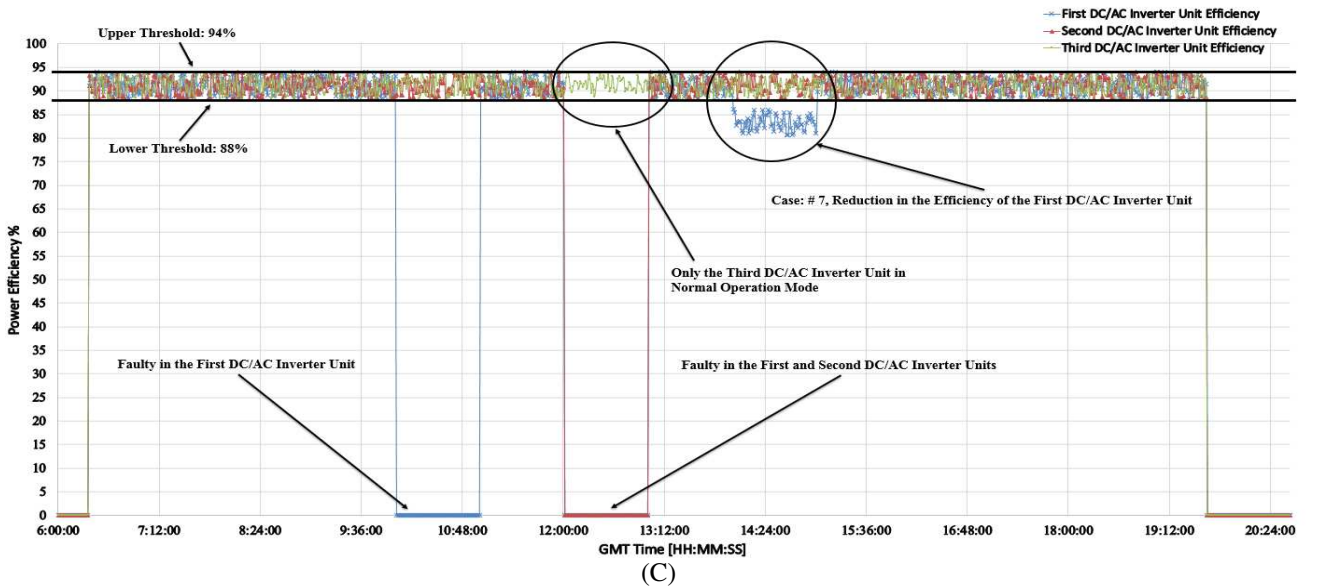
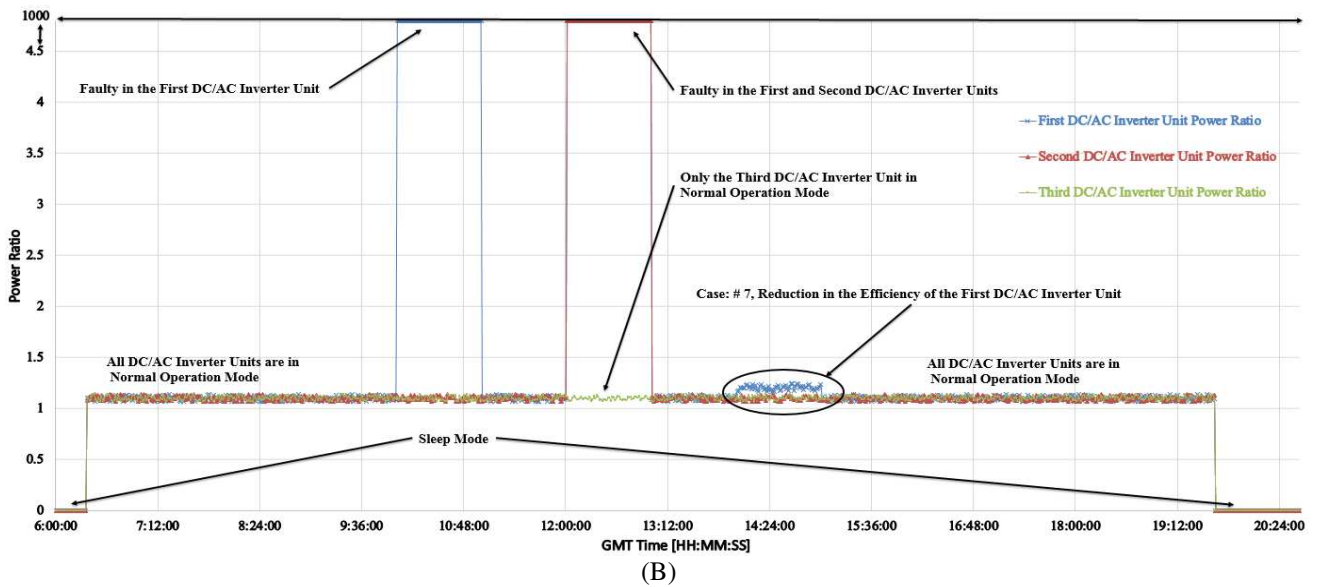
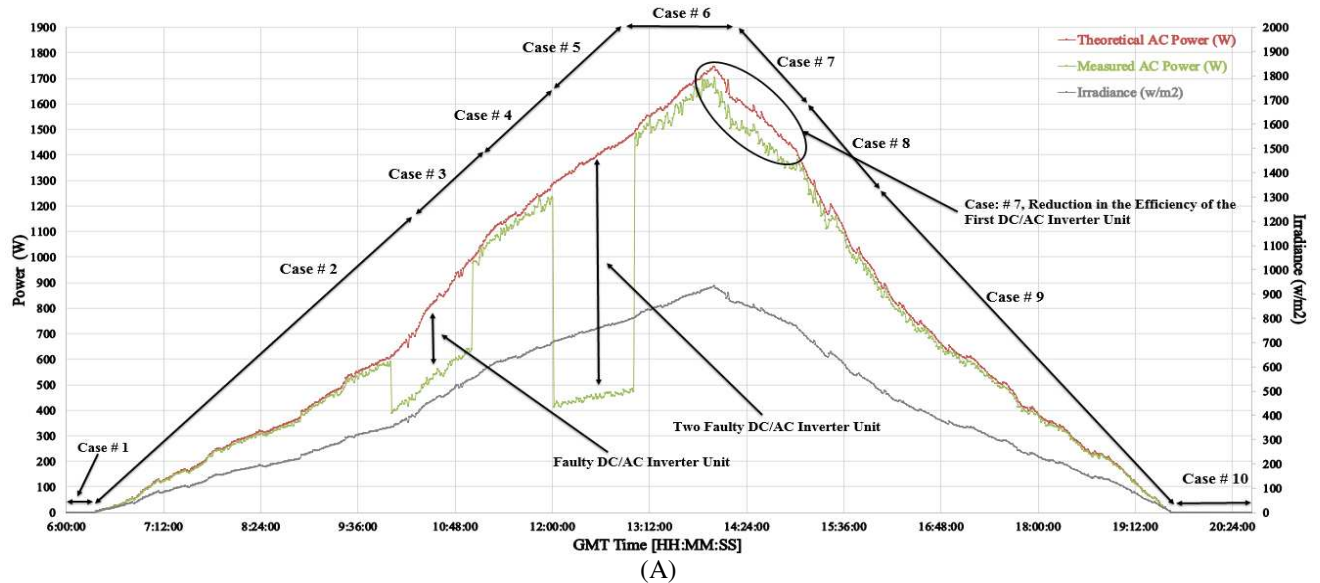


Fig. 12. Diagnosis the Faults Using Fault Detection Algorithm 2. (A) GCPV System Theoretical AC Power vs. Measured Output AC Power, (B) Power Ratio for All DC/AC Inverter Units, (C) Output Power Efficiency for all DC/AC Inverter Units

330 **4.5. Performance Evaluation of the Proposed PV Fault Detection Algorithm Based on Array Ages**

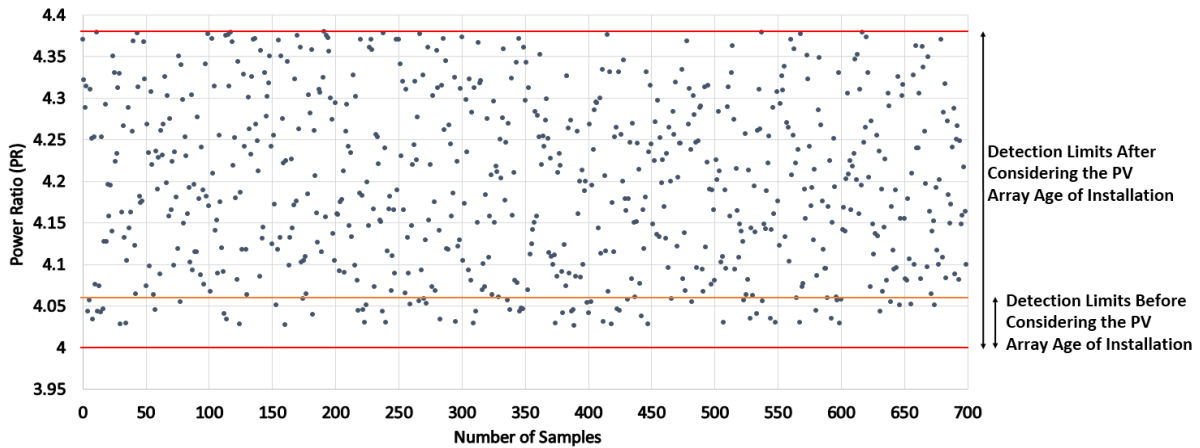
331 Since the examined PV modules used in the previous sections is new (installed 2 years ago), the proposed  
 332 PV detection algorithm was evaluated using another PV system as shows in Fig. 14, where the total PV  
 333 system capacity is equal to 0.52 kWp. The MPPT unit and DC/AC inverter are previously explained in  
 334 section 2. The PV modules are installed at the University of Huddersfield 11 years ago. Table 4 shows the  
 335 theoretical power ratio fault detection limits calculated using (5) for various case scenarios before  
 336 considering the age of the PV installation.

337 Fig. 13(A) shows the measured PR while disconnecting 3 PV modules (3 PV modules are inactive).  
 338 Using the detection limits obtained by (5), most of the measured PR samples are does not lie between the  
 339 detection limits since equation (5) does not contain the degradation rate of the PV array due to the PV  
 340 array age. Therefore, it is required to use (7) which has the value of the degradation rate for the PV  
 341 installation, where the new detection limits are presented in Table 4.

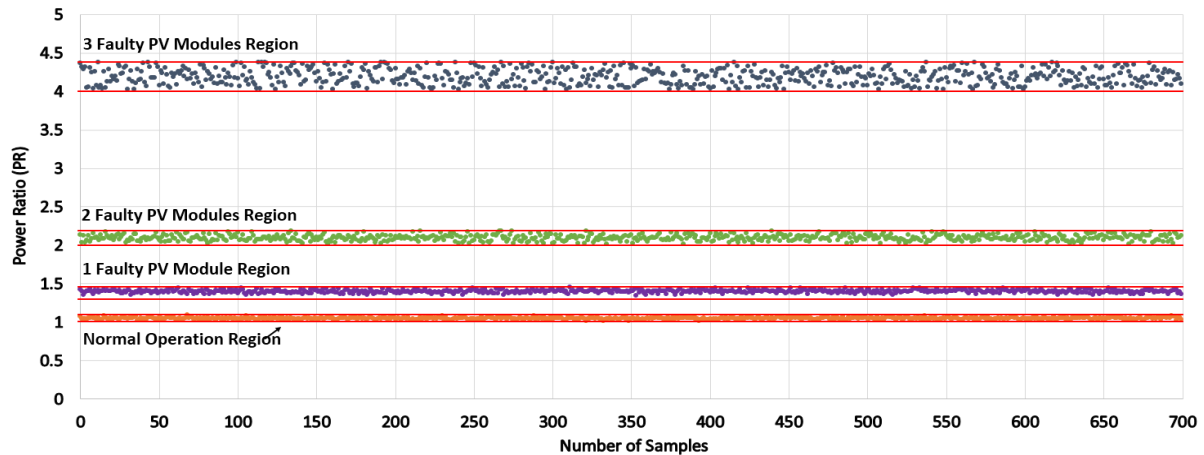
342 
$$PR = \frac{P_{theoretical}}{P_{measured} \times MPPT \text{ efficiency} \times (100 - \text{Accumulative PV Degredation Rate})} \quad (7)$$

343  
 344 Where the accumulative PV degradation rate is calculated using (8).

345 
$$\text{Accumulative PV Degredation Rate} = \text{PV Degredation rate per year} \times \text{PV Age of Instllation} \quad (8)$$



(A)



(B)

Fig. 13. Power Ratio Variations Obtained by the Second PV System. (A) PR Variations for 3 Faulty PV Modules, (B) PR Variations for all Examined Case Scenarios vs. Detection Limits Which are Explained in Table 4

346 Fig. 13(B) shows the measured PR values for several tests. The theoretical thresholds have been  
 347 calculated at a degradation rate equals to 0.67%/year. This rate ensure that all measured data lies within  
 348 the detection region of the power ratio as illustrated in Table 4. As a result, by using (8) the accumulative  
 349 degradation rate of the PV modules is equal to:

350 
$$\text{Accumulative PV Degredation Rate} = 0.67 \left( \frac{\text{degradation}}{\text{year}} \right) \times 11 (\text{PV Age of Instllation}) = 7.37$$

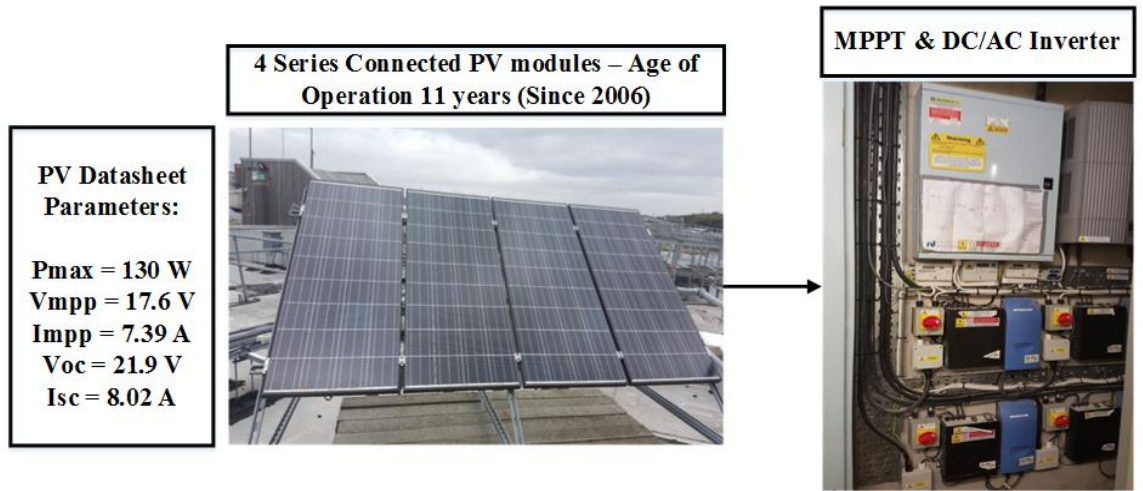


Fig. 14. Second Examined PV System Installed at the University of Huddersfield - Year of Installation is 2006

TABLE 4  
 THEORETICAL THRESHOLD CALCULATIONS USING THE EXAMINED PV SYSTEM SHOWN IN FIG. 13

Examined Case Scenario	Theoretical Thresholds Calculations Using (5) Before Considering the PV Array Age of Installation	Theoretical Thresholds Calculations Using (7) After Considering the PV Array Age of Installation
Normal Operation mode	$RR_{min} = \frac{130 \times 4}{130 \times 4} = 1$ $PR_{max} = \frac{130 \times 4}{130 \times 4 \times 98.5\%} = 1.015$	$RR_{min} = \frac{130 \times 4}{130 \times 4} = 1$ $PR_{max} = \frac{130 \times 4}{130 \times 4 \times 98.5\% \times (100 - 7.37)\%} = 1.096$
Faulty PV module	$RR_{min} = \frac{130 \times 4}{130 \times 3} = 1.3$ $PR_{max} = \frac{130 \times 4}{130 \times 3 \times 98.5\%} = 1.35$	$RR_{min} = \frac{130 \times 4}{130 \times 3} = 1.3$ $PR_{max} = \frac{130 \times 4}{130 \times 3 \times 98.5\% \times (100 - 7.37)\%} = 1.46$
2 Faulty PV modules	$RR_{min} = \frac{130 \times 4}{130 \times 2} = 2$ $PR_{max} = \frac{130 \times 4}{130 \times 2 \times 98.5\%} = 2.03$	$RR_{min} = \frac{130 \times 4}{130 \times 2} = 2$ $PR_{max} = \frac{130 \times 4}{130 \times 2 \times 98.5\% \times (100 - 7.37)\%} = 2.19$
3 Faulty PV modules	$RR_{min} = \frac{130 \times 4}{130 \times 1} = 4$ $PR_{max} = \frac{130 \times 4}{130 \times 1 \times 98.5\%} = 4.06$	$RR_{min} = \frac{130 \times 4}{130 \times 1} = 4$ $PR_{max} = \frac{130 \times 4}{130 \times 1 \times 98.5\% \times (100 - 7.37)\%} = 4.38$

351 **4.6. Discussion**

352 In order to test the effectiveness of the proposed parallel fault detection algorithm, the results obtained  
353 have been compared with the multiple fault detection algorithms presented in [10 and 12-14]. The  
354 comparison between the outputs given by our proposed algorithm and four recent fault detection methods  
355 are shown in Table 5.

356 It can be seen that, different case studies have been examined for each of the methods, and only the  
357 parallel fault detection algorithm (this work) can diagnose all the case studies that have been examined.  
358 None of the reviewed fault detection algorithms can identify hot spots and dust levels in GCPV systems.  
359 It is necessary, therefore, to carry out further work in these areas with a view to including the detection of  
360 these faults in a future generic advanced algorithm.

361 The proposed algorithm has used two ratios (VR and PR) which are similar to the power and voltage  
362 ratios described by Silvestre et al [22]. However, the proposed approach used in [27] dose not detect any  
363 failures in the AC side of the examined GCPV systems. Similar power and voltage ratios has been reused  
364 by A. Karabiber et al [10], but this algorithm is using the estimation of the hourly solar radiation using  
365 GISTEL model which has been improved by a fuzzy logic rules.

366 The combination between the DC side and AC side power ratio can be used to detect possible faults in the  
367 GCPV plant as described by W. Chine et al [12]. This approach is different than the proposed algorithm  
368 used in this paper by the following:

- 369 1. This paper divided the DC and AC side power ratios into two different indicators, which makes  
370 the algorithm easier to reuse with larger PV installations later on.
- 371 2. This paper shows how to detect faulty bypass diode with partial shading conditions effect the  
372 GCPV system. However, [12] does not have this feature as illustrated in Table 5.

373 Nowadays, some articles use artificial intelligent networks (ANN) in order to detect faults in GCPV  
374 systems. W. Chine et al [13] demonstrate an ANN fault detection approach used with PV systems. The  
375 approach is focused on faulty conditions such as inversed bypass diodes, shunted bypass diodes and short  
376 circuit fault in bypass diodes. Only a faulty bypass diode with partial shading effect is presented by this  
377 paper.

378 Several statistical analysis techniques have been used to detect possible faults in GCPV plants. A  
379 regression algorithm for diagnosis faults in PV generators has been illustrated by W. Rezgui et al [28].  
380 However, M. Dhimish et al [29] used another statistical analysis technique called t-test, which is similar  
381 to the work presented in this paper. Some other approaches used standard divination ( $\sigma$ ) limits, either  $\pm 3\sigma$   
382 or  $\pm \sigma$  such as [10, 12 and 16].

383 In this paper, multiple DC/AC inverter units have been used. Each inverter is used with separate PV  
384 string. However, it is possible to generalize the presented algorithm (algorithm 2) to be used with a  
385 centralized inverter for a GCPV structure [32] by adding the theoretical limits of the DC/AC inverter and  
386 then calculating the power ratio based on the total input power of the PV system.

387 The parallel fault detection algorithm presented in this work has some disadvantages such as:

- 388 1. The algorithm cannot detect faults occurring in multiple bypass diodes in the PV system.
- 389 2. Algorithm 1 detects faults in the DC side of the PV systems, however, this algorithm is based on  
390 the analysis of the power and voltage which are measured by the internal sensor of the MPPT  
391 unit, and therefore, the algorithm accuracy depends on the instruments used in the PV installation.

392 The main contribution of this work is the variation of the minimum and maximum power and voltage  
 393 ratios which can be evaluated using (5-6). The main finding of the proposed algorithm 1 is shown in Fig.  
 394 15. The x-axis presents PR and y-axis shows VR variations. This figure shows that when the PR is  
 395 between 1 and 1.015, the GCPV plant is operating at normal mode despite the value of the VR. Moreover,  
 396 the SIR region is used to identify the partial shading condition effects the PV systems.

397 The proposed parallel fault detection algorithm contains the variations of the power and the voltage of the  
 398 PV system. However, in the series-parallel PV array configuration system architecture the current ratio  
 399 must be included in the mathematical calculations [30]. Moreover, in the parallel PV array configuration  
 400 the voltage ratio must be replaced by the current ratio since the voltage does not change significantly  
 401 during faulty conditions.

402 Virtual Instrumentation (VI) LabVIEW software is a useful tool which has been used widely for  
 403 monitoring and analyzing the performance of PV systems [15, 31 and 32]. Therefore, the design of the  
 404 parallel fault detection algorithm has been implemented using virtual instrumentation LabVIEW software.  
 405 Appendix B, presents a mixed signal graph showing voltage ratio, DC power ratio, AC power ratio and  
 406 weather station data such as:

- 407 1. Solar Irradiance
- 408 2. Temperature
- 409 3. Humidity

410 The GCPV plant theoretical and measured output performance indicators for the DC-Side and AC-Side  
 411 are shown in appendix B. Also appendix B shows a brief illustration of the error which has been detected  
 412 by the algorithm in both DC and AC sides.

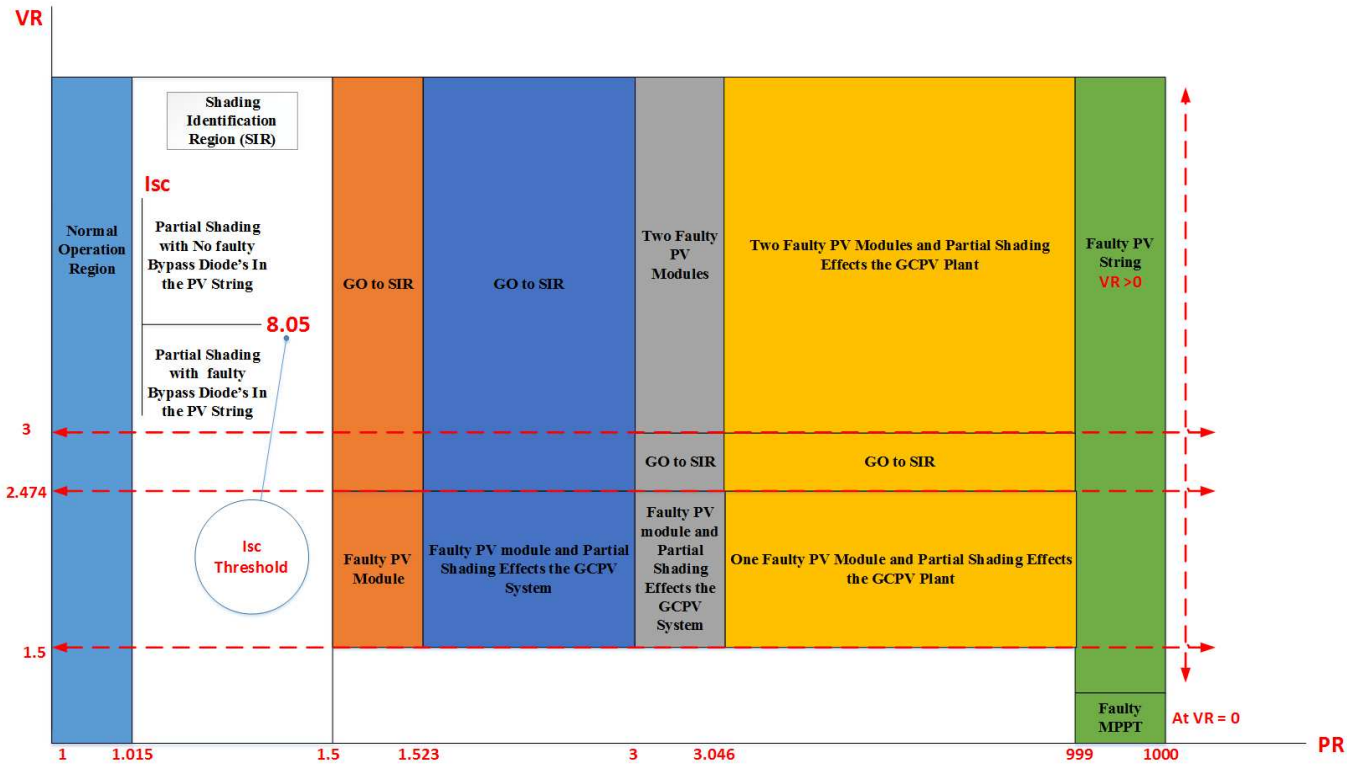


Fig. 15. PR vs. VR Based on the Analysis of Fault Detection Algorithm 1

TABLE 5  
COMPARATIVE RESULTS BETWEEN THE PROPOSED ALGORITHM AND SEVERAL FAULT DETECTION METHODS

Case Study	Proposed Algorithm	Ref. [14]	Ref. [13]	Ref. [16]	Ref. [12]	Ref. [10]
Month / Year of the Study	2017	August 2016	January 2016	October 2015	December 2014	February 2014
Fault Detection Algorithm Approach	T-test Statistical Technique	T-test Statistical Technique	I-V Curve Characteristics and ANN	Standard Deviation Statistical Technique	Mathematical Ratios	± Standard Deviation and Fuzzy Logic
Software Used in the Study	LabVIEW	LabVIEW	MATLAB/SIMULINK	Not Mentioned	MATLAB/SIMULINK	MATLAB/SIMULINK
Faulty PV Module in a PV String	√	√	√	×	√	√
Faulty Strings in a GCPV Plant	√	√	√	×	√	√
Faulty MPPT Unit	√	√	×	×	√	×
Faulty DC/AC Inverter Unit	√	×	×	√	√	×
Partial Shading Effect	√	√	√	×	√	√
Faulty Bypass Diodes	√	×	√	×	×	×
Faults in the Data Acquisition	√	√	×	√	√	√

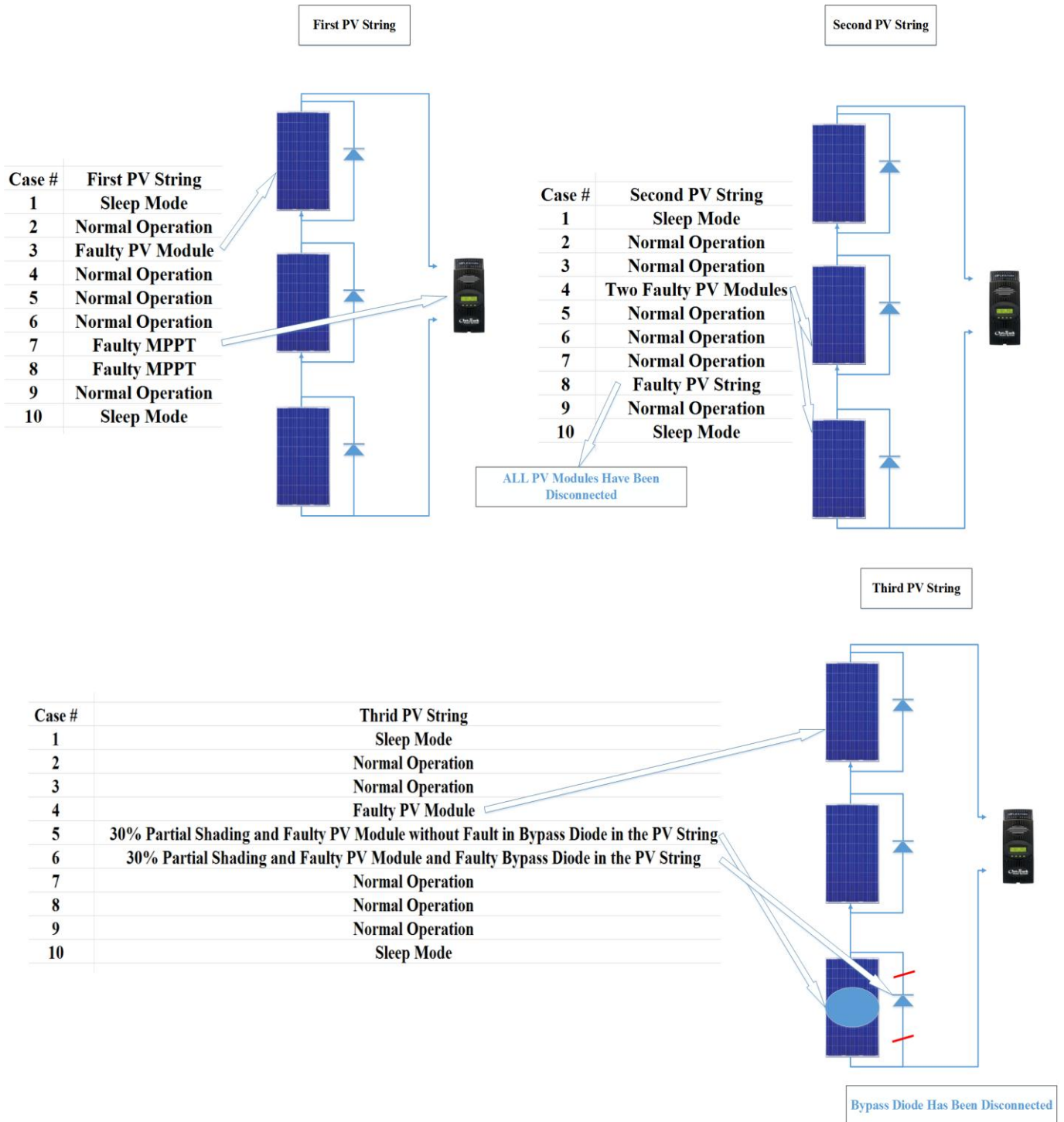
## 413 5. CONCLUSION

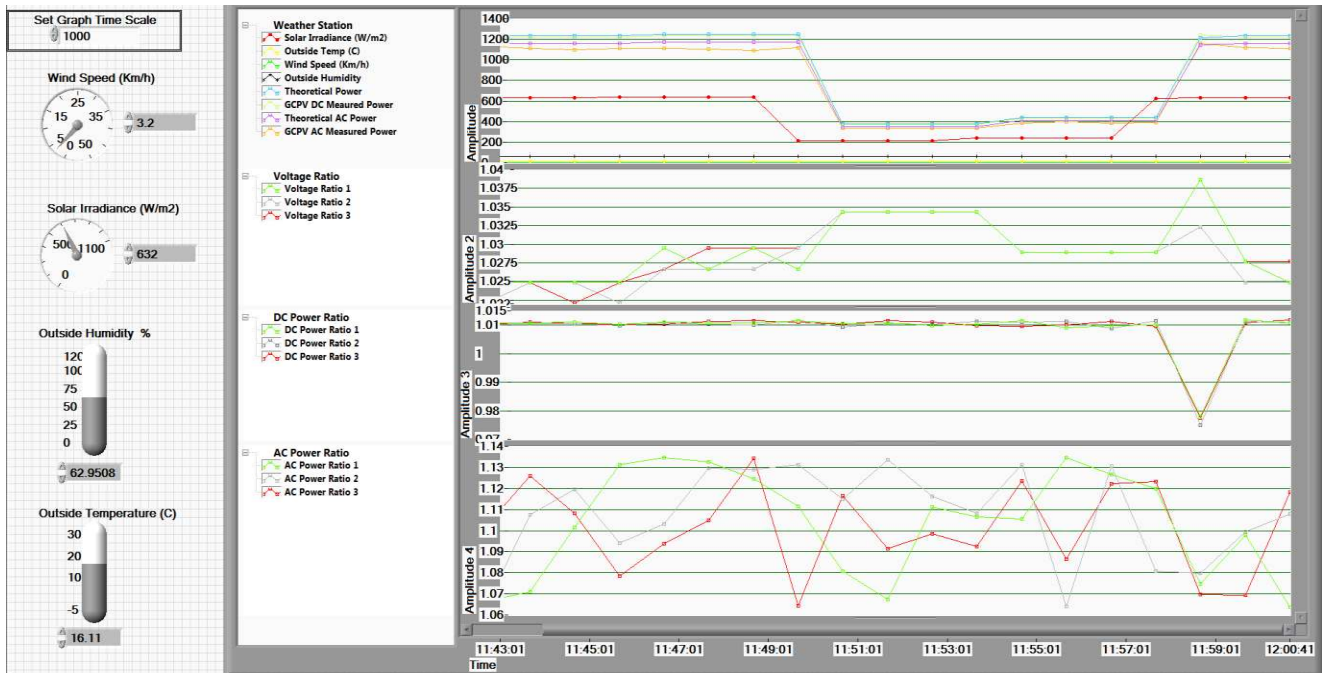
414 A parallel fault detection algorithm for a grid-connected photovoltaic (GCPV) plant based on a t-test  
415 statistical approach is proposed and verified using a 1.98 and 0.52 kWp GCPV plants. The parallel  
416 detection algorithm contains two sub algorithms. The first is used to facilitate the detection of faults on  
417 the DC-side of the GCPV system, while the second facilitates the detection of two different fault types on  
418 the AC-side of the GCPV plant.

419 In order to identify failures in the GCPV system, we have defined two indicators namely, power ratio  
420 (PR) and voltage ratio (VR). By using both ratios it is possible to determine the fault type, time and the  
421 location of the fault. The graphical user interface (GUI) was created to monitor the status of the existing  
422 system using virtual instrumentation (VI) LabVIEW software.

423 A novel contribution of this research is the use of a new statistical approach to identify failures on the DC  
424 and AC sides of the GCPV plant based on real-time, long-term field data measurements. Additionally the  
425 performance of the PV detection algorithm was evaluated using a two difference PV installations.

426 In the future, it is intended to create a generic fault detection algorithm to detect multiple faults in the  
427 GCPV systems based on artificial intelligence machine learning techniques. Also, it is possible to enhance  
428 the parallel fault detection algorithm by detecting more faults occurring in the PV systems such as the  
429 change in the series resistance due to faulty conditions affecting the PV panels.





Weather Station Data			
Sample Number	G (Irradiance W/m <sup>2</sup> )	Temperature (C)	Loop Count
113	632	16.11	0

FIRST ARRAY STATUS		First Array	
G (Irradiance W/m <sup>2</sup> )	632	P1	P2 P3
Temperature (C)	16.11	I1	I2 I3
Irradiance	Temp	V1	V2 V3
		First String Power Ratio	1.00885
		First String Voltage Ratio	1.02206
		First String Current Ratio	0.986423
		First String Efficiency %	99.1225
		Isc Measured	8.16

FIRST ARRAY STATUS		Second Array	
G (Irradiance W/m <sup>2</sup> )	632	P1	P2 P3
Temperature (C)	16.12	I1	I2 I3
Irradiance	Temp	V1	V2 V3
		Second String Power Ratio	1.01068
		Second String Voltage Ratio	1.02488
		Second String Current Ratio	0.982291
		Second String Efficiency %	98.9437
		Isc Measured	8.177

THIRD ARRAY STATUS		Third Array	
G (Irradiance W/m <sup>2</sup> )	632	P1	P2 P3
Temperature (C)	16.17	I1	I2 I3
Irradiance	Temp	V1	V2 V3
		Third String Power Ratio	1.00965
		Third String Voltage Ratio	1.02206
		Third String Current Ratio	0.986423
		Third String Efficiency %	99.0447
		Isc Measured	8.167

DC-SIDE	
First Array	Error Detection in the First PV array NORMAL OPERATION
Second Array	Error Detection in the Second PV array NORMAL OPERATION
Third Array	Error Detection in the Third PV array NORMAL OPERATION

AC-SIDE				
First DC/AC Inverter Power Ratio	1.09309	First DC/AC Inverter Power Efficiency %	91.4836	Error Detection in the First DC/AC Inverter NORMAL OPERATION DC/AC INVERTER UNIT
Second DC/AC Inverter Power Ratio	1.09332	Second DC/AC Inverter Power Efficiency %	91.4647	Error Detection in the Second DC/AC Inverter NORMAL OPERATION DC/AC INVERTER UNIT
Third DC/AC Inverter Power Ratio	1.10549	Third DC/AC Inverter Power Efficiency %	90.4578	Error Detection in the Third DC/AC Inverter NORMAL OPERATION DC/AC INVERTER UNIT

GCPV Output Performance			
Theoretical DC Power (W)	1234.7	GCPV DC Measured Power (W)	1222.81
Theoretical AC Power (W)	1149.44	GCPV AC Measured Power (W)	1114.41

432

## References

- 433 [1] Ondraczek, J. (2014). Are we there yet? Improving solar PV economics and power planning in developing  
434 countries: The case of Kenya. *Renewable and Sustainable Energy Reviews*, 30, 604-615.
- 435 [2] Khamis, A., Shareef, H., Bizkevelci, E., & Khatib, T. (2013). A review of islanding detection techniques for  
436 renewable distributed generation systems. *Renewable and sustainable energy reviews*, 28, 483-493.
- 437 [3] Qi, J., Zhang, Y., & Chen, Y. (2014). Modeling and maximum power point tracking (MPPT) method for PV  
438 array under partial shade conditions. *Renewable Energy*, 66, 337-345.
- 439 [4] Saravanan, S., & Babu, N. R. (2016). Maximum power point tracking algorithms for photovoltaic system—A  
440 review. *Renewable and Sustainable Energy Reviews*, 57, 192-204.
- 441 [5] Potnuru, S. R., Pattabiraman, D., Ganesan, S. I., & Chilakapati, N. (2015). Positioning of PV panels for  
442 reduction in line losses and mismatch losses in PV array. *Renewable Energy*, 78, 264-275.
- 443 [6] Eke, R., & Demircan, C. (2015). Shading effect on the energy rating of two identical PV systems on a building  
444 façade. *Solar Energy*, 122, 48-57.
- 445 [7] Fathy, A. (2015). Reliable and efficient approach for mitigating the shading effect on photovoltaic module based  
446 on Modified Artificial Bee Colony algorithm. *Renewable Energy*, 81, 78-88.
- 447 [8] Mejia, F., Kleissl, J., & Bosch, J. L. (2014). The effect of dust on solar photovoltaic systems. *Energy*  
448 *Procedia*, 49, 2370-2376.
- 449 [9] Jelle, B. P. (2013). The challenge of removing snow downfall on photovoltaic solar cell roofs in order to  
450 maximize solar energy efficiency—Research opportunities for the future. *Energy and Buildings*, 67, 334-351.
- 451 [10] Karabiber, A., Keles, C., Kaygusuz, A., & Alagoz, B. B. (2013). An approach for the integration of renewable  
452 distributed generation in hybrid DC/AC microgrids. *Renewable energy*, 52, 251-259.
- 453 [11] Tadj, M., Benmouiza, K., Cheknane, A., & Silvestre, S. (2014). Improving the performance of PV systems by  
454 faults detection using GISTEL approach. *Energy conversion and management*, 80, 298-304.
- 455 [12] Takashima, T., Yamaguchi, J., Otani, K., Oozeki, T., Kato, K., & Ishida, M. (2009). Experimental studies of  
456 fault location in PV module strings. *Solar Energy Materials and Solar Cells*, 93(6), 1079-1082.
- 457 [13] Chine, W., Mellit, A., Pavan, A. M., & Kalogirou, S. A. (2014). Fault detection method for grid-connected  
458 photovoltaic plants. *Renewable Energy*, 66, 99-110.
- 459 [14] Chine, W., Mellit, A., Lughì, V., Malek, A., Sulligoi, G., & Pavan, A. M. (2016). A novel fault diagnosis  
460 technique for photovoltaic systems based on artificial neural networks. *Renewable Energy*, 90, 501-512.
- 461 [15] Dhimish, M., & Holmes, V. (2016). Fault detection algorithm for grid-connected photovoltaic plants. *Solar*  
462 *Energy*, 137, 236-245.
- 463 [16] Platon, R., Martel, J., Woodruff, N., & Chau, T. Y. (2015). Online Fault Detection in PV Systems. *Sustainable*  
464 *Energy*, *IEEE Transactions on*, 6(4), 1200-1207.
- 465 [17] Kim, K. A., Seo, G. S., Cho, B. H., & Krein, P. T. (2016). Photovoltaic Hot-Spot Detection for Solar Panel  
466 Substrings Using AC Parameter Characterization. *IEEE Transactions on Power Electronics*, 31(2), 1121-1130.
- 467 [18] Silvestre, S., Kichou, S., Chouder, A., Nofuentes, G., & Karatepe, E. (2015). Analysis of current and voltage  
468 indicators in grid connected PV (photovoltaic) systems working in faulty and partial shading conditions. *Energy*, 86,  
469 42-50.

- 470 [19] McEvoy, A., Castaner, L., Markvart, T., 2012. Solar Cells: Materials, Manufacture and Operation. Academic  
471 Press.
- 472 [20] Sera, D., Teodorescu, R., & Rodriguez, P. (2007). PV panel model based on datasheet values. Paper presented  
473 at the 2392-2396. doi:10.1109/ISIE.2007.4374981
- 474 [21] So, J. H., Jung, Y. S., Yu, G. J., Choi, J. Y., & Choi, J. H. (2007). Performance results and analysis of 3kW  
475 grid-connected PV systems. *Renewable Energy*, 32(11), 1858-1872.
- 476 [22] Silvestre, S., Chouder, A., & Karatepe, E. (2013). Automatic fault detection in grid connected systems. *Solar  
477 Energy*, 94, 119-127.
- 478 [23] Kouro, S., Leon, J. I., Vinnikov, D., & Franquelo, L. G. (2015). Grid-connected photovoltaic systems: An  
479 overview of recent research and emerging PV converter technology. *IEEE Industrial Electronics Magazine*, 9(1), 47-  
480 61.
- 481 [24] Díez-Mediavilla, M., Dieste-Velasco, M. I., Rodríguez-Amigo, M. C., García-Calderón, T., & Alonso-Tristán,  
482 C. (2014). Performance of grid-tied PV facilities based on real data in Spain: central inverter versus string  
483 system. *Energy Conversion and Management*, 86, 1128-1133.
- 484 [25] Planas, E., Andreu, J., Gárate, J. I., de Alegría, I. M., & Ibarra, E. (2015). AC and DC technology in  
485 microgrids: A review. *Renewable and Sustainable Energy Reviews*, 43, 726-749.
- 486 [26] El-Dein, M. S., Kazerani, M., & Salama, M. M. A. (2013). Optimal photovoltaic array reconfiguration to  
487 reduce partial shading losses. *IEEE Transactions on Sustainable Energy*, 4(1), 145-153.
- 488 [27] Silvestre, S., da Silva, M. A., Chouder, A., Guasch, D., & Karatepe, E. (2014). New procedure for fault  
489 detection in grid connected PV systems based on the evaluation of current and voltage indicators. *Energy  
490 Conversion and Management*, 86, 241-249.
- 491 [28] Rezgui, W., Mouss, N. K., Mouss, L. H., Mouss, M. D., & Benbouzid, M. (2014, March). A Regression  
492 Algorithm for the Smart Prognosis of a Reversed Polarity Fault in a Photovoltaic Generator. In *IEEE ICGE  
493 2014* (pp. 134-138).
- 494 [29] Dhimish, M., Holmes, V., & Dales, M. (2016, November). Grid-connected PV virtual instrument system  
495 (GCPV-VIS) for detecting photovoltaic failure. In *Environment Friendly Energies and Applications (EFEA), 2016  
496 4th International Symposium on* (pp. 1-6). IEEE.
- 497 [30] Obi, M., & Bass, R. (2016). Trends and challenges of grid-connected photovoltaic systems—A  
498 review. *Renewable and Sustainable Energy Reviews*, 58, 1082-1094.
- 499 [31] Chouder, A., Silvestre, S., Taghezouit, B., & Karatepe, E. (2013). Monitoring, modelling and simulation of PV  
500 systems using LabVIEW. *Solar Energy*, 91, 337-349.
- 501 [32] M. Dhimish, V. Holmes and B. Mehrdadi, "Grid-connected PV monitoring system (GCPV-MS)," *2016 4th  
502 International Symposium on Environmental Friendly Energies and Applications (EFEA)*, Belgrade, Serbia, 2016,  
503 pp. 1-6. doi: 10.1109/EFEA.2016.7748772